

Hydroxyapatite Formation in a Single-Stage Anammox-Based Batch Treatment System: Reactor Performance, Phosphorus Recovery, and Microbial Community

Albert Magrí,* Emma Company, Frederic Gich, and Jesús Colprim

Cite This: *ACS Sustainable Chem. Eng.* 2021, 9, 2745–2761

Read Online

ACCESS |



Metrics & More



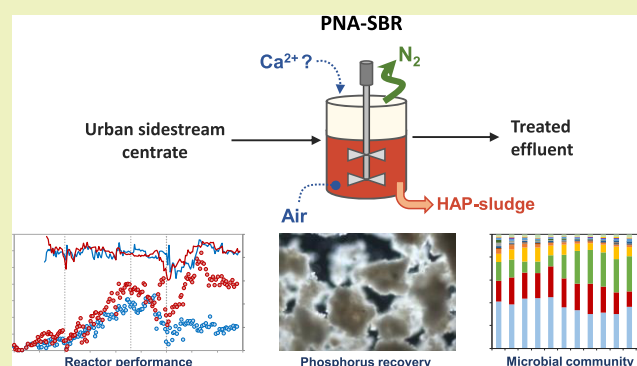
Article Recommendations



Supporting Information

ABSTRACT: Simultaneous ammonium–nitrogen ($\text{NH}_4^+\text{-N}$) removal and orthophosphate–phosphorus ($\text{PO}_4\text{-P}$) biomineralization was studied in two granular sludge sequencing batch reactors treating urban sidestream centrate through the one-stage partial nitritation–anaerobic ammonium oxidation (anammox) process. By adding an external source of calcium, concomitant conversion rates of up to 0.32 g $\text{NH}_4^+\text{-N}/(\text{L}\cdot\text{days})$ and 12 mg $\text{PO}_4\text{-P}/(\text{L}\cdot\text{days})$ were measured while reaching water-phase removal efficiencies of ca. 80% of the $\text{NH}_4^+\text{-N}$ and 70% of the $\text{PO}_4\text{-P}$ loaded. The mineral cores formed inside the granules were mostly composed of hydroxyapatite (HAP), which is a recoverable phosphate salt. Yet, the high mineralization of the sludge and its excessive purge from the bioreactor limited the microbial activity in the long term. In this sense, the densest granules, accumulated at the bottom of the bioreactor, were the most susceptible to being harvested because they were the richest in HAP, but at the same time, they contained the highest percentages of anammox bacteria.

KEYWORDS: calcium phosphate, precipitated phosphate salt, deammonification, digester supernatant, high-throughput sequencing, *Ca. Kuenenia stuttgartiensis*

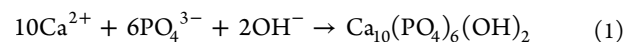


INTRODUCTION

Phosphorus (P) is an essential element for all living organisms. This nutrient is absolutely necessary for sustaining agri-food production, and its demand rises alongside the growth of the global population.¹ Currently, mined phosphate rock (i.e., apatite-type ores) is the primary source of P, but this is a finite resource, which is unevenly distributed around the world.² The European Union (EU) depends on the import of P, and it has identified phosphate rock and P as 2 of the 27 critical raw materials having high importance to the EU economy and having a high risk associated with their supply.³

The discharge of improperly treated sewage and P excess into aquatic ecosystems causes the deterioration of water quality due to the proliferation of algae and eutrophication.⁴ Otherwise, according to the circular economy paradigm, wastewater is a renewable source of P, available at the local scale. Hence, wastewater treatment offers a good opportunity to exploit new ways to produce P-related feedstock aiming at a more sustainable development while preventing pollution. Different methods can be applied in wastewater treatment plants (WWTPs) to achieve P recovery (e.g., crystallization from sewage and internal aqueous streams, extraction from sludge using wet-chemical techniques, transformation from ashes or biochar produced from sludge thermal processing, etc.).⁵ Among them, the crystallization and precipitation of

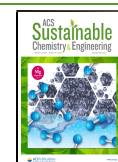
low-soluble salts are commonly used, based on the combination of the dissolved orthophosphate (PO_4) with a metal ion, e.g., calcium (Ca), magnesium (Mg), or iron (Fe). Broadly, in view of biological treatment, phosphate precipitation can be accomplished according to upstream, concomitant, or downstream strategies.⁶ Regarding the product finally obtained, magnesium phosphates (MgP) such as struvite (magnesium ammonium phosphate (MAP)) are frequently considered as an efficient slow-release fertilizer for crops,⁷ whereas calcium phosphates (CaP) such as hydroxyapatite (HAP) offer broader industrial applications beyond fertilizers since the composition is similar to mined phosphate rock.⁸ The equation for the crystallization of HAP ($\text{Ca}_{10}(\text{PO}_4)_6(\text{OH})_2$), a mineral containing 18.5 wt % P, is as follows: (eq 1)⁹



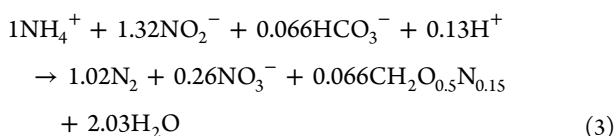
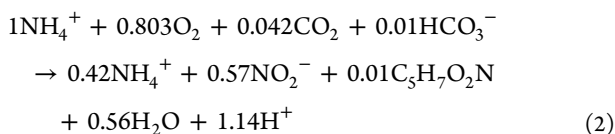
Received: November 3, 2020

Revised: January 19, 2021

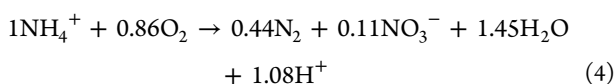
Published: February 9, 2021



Owing to the significant enhancement in the energy balance achievable with respect to other conventional biotechnologies, completely autotrophic nitrogen (N) removal (i.e., the partial nitrification–anammox (PNA) process) is an appealing alternative for treating the N-rich sidestream centrates produced in urban WWTPs.¹⁰ This process is based on the coupling of partial nitrification (PN), targeting partial aerobic ammonium (NH_4^+) oxidation to nitrite (NO_2^-) without nitrate formation (NO_3^-) (eq 2),¹¹ and anaerobic ammonium oxidation (anammox, A), in which ammonium and nitrite are converted in the absence of oxygen to dinitrogen gas (N_2) with small nitrate production (eq 3).¹²



The sidestream centrate obtained after centrifuging anaerobically digested sludge for its dewatering contains low levels of biodegradable organic carbon. If no treatment is considered, then this centrate is returned back to the headworks of the WWTP, contributing in a small proportion to the flow entering the plant, but to a larger extent to the amount of nutrients loaded in the mainstream. The PNA-based treatment of this centrate favors the energy self-sufficiency of the WWTP, mostly because of the diminished energy demand for aeration and the feasibility for increasing the recovery of renewable energy in the form of biogas through anaerobic digestion. Its application, thus, can help in reducing the environmental impact and in improving sustainability in wastewater treatment.^{13,14} In this context, the PNA process is frequently engineered in single-stage systems¹⁵ according to eq 4 (biomass not included). Granular sludge sequencing batch reactors (SBRs) are commonly considered, running under oxygen (O_2) mass transfer limitation due to low-intensity aeration. Oxygen is a substrate for nitrification but also inhibits reversibly the anammox process. This fact makes aeration control of primary importance to maximize the N-removal rate and efficiency¹⁶ owing to the delicate equilibrium existing between both bioprocesses, with minimal nitrification (i.e., aerobic nitrite oxidation to nitrate). Aerobic ammonium-oxidizing bacteria (AOB) are supposed to be the dominant microorganisms in the outer layer of the granules, whereas anammox bacteria (AnAOB) dominate the inner part. Such a microbial distribution results in a local pH-value gradient along the granule radius, with higher pH values in the core.¹⁷ Alkalinity consumption (i.e., mostly comprising the inorganic carbon system) and pH-value diminution (acidification) in the bulk liquid are other collateral consequences of the PNA process. These parameters play a primary role when targeting phosphate precipitation.



Biologically induced phosphate mineralization has already been proposed as a promising alternative for recovering P from

sidestream centrate, either as MgP^{18} or as $\text{CaP}^{19,20}$. Biomediated precipitation involves the reaction between extracellular ions and metabolic products released across or into the cell wall. Recent works integrating anammox and CaP-precipitation reactions evidenced the feasibility of the formation of a dense HAP core wrapped by an external biofilm.^{21,22} As a consequence, a highly mineralized sludge is produced within the bioreactor. Once this sludge is harvested, the high P content makes it an interesting resource for subsequent valorization. Specifically using a single-stage PNA granular system, Johansson et al.¹⁹ (SBR at 25 °C) treated real urban sidestream centrate under loading rates of 0.31 g N/(L-days) and 18 mg P/(L-days), achieving 66% N removal and HAP crystallization without adding chemicals; more recently, Guo and Li²³ (airlift reactor at 25 °C) worked with synthetic wastewater reaching N-removal rates as high as 1.2 g N/(L-days) and 83% P removal from water. Similar to the anammox systems described above, local gradients of pH value and constituent ion concentration have also been described as the driving forces triggering the enrichment of CaP in granules from other aerobic²⁴ and anaerobic²⁵ wastewater treatment applications.

Following the previous work on this topic carried out by the LEQUIA research group,¹⁹ the objective of this study is to obtain further insights into simultaneous N removal through the PNA process and P mineralization by HAP crystallization. To do so, two PNA SBRs have been operated in parallel processing real urban sidestream centrate. Particularly, the focus of this study is the analysis of the appropriate conditions favoring the performance of the process, including the supply of an external source of Ca for enhancing P recovery. To characterize the evolution of the microbial community involved in such a process, the dynamics of the prokaryotes growing within the granular bioreactors is analyzed by 16S ribosomal ribonucleic acid (rRNA) gene high-throughput sequencing.

MATERIALS AND METHODS

Sludge Source. The sludge used as inoculum was collected from a full-scale leachate treatment plant in a landfill site (CORSA, Reus, Spain). This facility uses a two-stage system that consists of two SBRs connected in series, where PN and anammox are operated individually.²⁶ On the sampling day, the leachate being processed was characterized as follows: pH, 8.3; conductivity, 35 mS/cm; alkalinity, 7.8 g CaCO_3 /L; chemical oxygen demand, 4.1 g O_2 /L; and NH_4^+ , 1.6 g N/L. Mixed liquors from both bioreactors (which were running at ca. 30 °C) were collected separately and, after arriving at the lab, blended together in two twin SBRs at a PN/anammox ratio of 5:10 L. After allowing the sludge to settle, and subsequent supernatant withdrawal, the final reactor volume was adjusted to 10 L, resulting in a total suspended solids (TSS) content of 0.88 g/L (98% as volatile suspended solids, VSS). At this point, both bioreactors started running cyclically.

Urban Sidestream Centrate. The urban sidestream centrate was collected after centrifugation at Terri WWTP (Cornellà de Terri, Catalonia, Spain) regularly every 3–4 weeks for a period longer than 1 year. After arriving at the lab, before its final storage and further processing, the centrate was naturally decanted for about 1 day to discard the eventual presence of suspended solids. A detailed characterization of this decanted centrate is given in Table S1.

Experimental Setup and Operational Conditions Applied. The single-stage PNA process was operated in two SBRs running in parallel, named SBR1 and SBR2, for approximately 15 months (from December 2018 to February 2020). Further details about the experimental setup, which was modified after Johansson et al.,¹⁹ are

Table 1. Process Performance in the PNA SBRs throughout the Experimental Period^a

parameter	phase I		phase II		phase III		phase IV	
	SBR1	SBR2	SBR1	SBR2	SBR1	SBR2	SBR1	SBR2
time length (days)	100		130		70		140	
aeration ($L_{\text{air}}/(L \cdot \text{days})$)	3–7	2–8	5–40	6–27	14–40	20–26	7–27	8–42
oxic reaction time (% of cycle)	73–83	73–83	73–88	73–88	89	89	61–82	80–89
hydraulic residence time (days)	≥ 11.4	≥ 7.4	2.9–17	2.2–25	2.2–4.9	1.4–3.2	3.1–13.7	1.4–2.9
metal ion addition ^b (mg/(L·days))	0	0	0	0	0–38	21–73	0–24	0
N loading rate (g $\text{NH}_4^+ \text{-N}/(L \cdot \text{days})$)	0–0.09	0–0.13	0.06–0.35	0.05–0.48	0.17–0.40	0.27–0.53	0.06–0.25	0.28–0.62
P loading rate (mg $\text{PO}_4\text{-P}/(L \cdot \text{days})$)	0–6	0–2	1–46 ^c	1–24	8–23	9–34	3–12	8–32
N conversion efficiency (% of NH_4^+)	67–96	63–99	78–91	71–92	80–89	72–86	66–94	61–93
P-uptake efficiency (PUE) (% of PO_4)	n.d. ^d	n.d.	0–45	n.d.	32–83	n.d.	46–88	n.d.
specific N conversion rate (mg $\text{NH}_4^+ \text{-N}/(g \text{ VSS} \cdot \text{days})$)	22–51	22–84	60–116	69–148	62–102	101–115	45–83	86–135

^aReported values are means of the three closest values available in the experimental phase being characterized. ^bMetal ions added in the bioreactors: Ca^{2+} in SBR1 and Mg^{2+} in SBR2. ^cAn external chemical phosphate source was added to the centrate used as feeding in SBR1 in phase II. ^dn.d.: not detected.

given in the Supporting Information. The process temperature was controlled at 25 ± 2 °C. Air was supplied through a solenoid valve and a gas mass flow controller (targeted airflow rate selected manually). As an additional safety factor, air supply was momentarily interrupted if the concentration of dissolved oxygen in the bulk liquid exceeded a set-point value (typically 0.3 mg O_2/L). The bioreactors ran according to cycles lasting 6 h throughout the experimental period, resulting in four cycles per day. However, different feeding strategies, external reagent supplies, and operational parameter values were considered during this time. The experimental period was divided into four different phases: phase I (days 0–100, 100 days), phase II (days 101–230, 130 days), phase III (days 231–300, 70 days), and phase IV (days 301–440, 140 days). In phase I (startup of the PNA process) and phase II (consolidation of the PNA process), one working cycle was scheduled as 9–10 repeated sequences of aerated feeding and reaction (each individual sequence lasting 29–31.5 min), followed by an anoxic reaction period (35–89 min), settling (15 → 5 min), and withdrawn (5 min). The absence of nitrite accumulation in the SBRs was verified by the end of a cycle on a daily basis by means of a ready-to-use kit. Increases in the airflow rate, and in the N loading rate (NLR) applied, were decided individually according to the fulfillment of this criterion. The NLR was raised by increasing the feeding pump inflow rate, or by lengthening the feeding, while maintaining constant the total length of each aerobic sequence. The pH within the bioreactors was only monitored, freely evolving according to the running conditions (7.0–7.8), but not controlled to a given set-point. A synthetic source of P (i.e., phosphate solution) was added to the centrate fed to SBR1 to increase the phosphate loading rate (PLR) applied. In phase III (cation supply to induce P precipitation), the configuration of the aerated periods (including feeding and reaction) was switched from a fixed-time schedule without pH control to a pH-based dynamic autoregulation. Moreover, a synthetic source of a metal cation was directly added to the SBRs at the beginning of the cycle by means of an additional pump (i.e., added by drip from the top of the bioreactor during the first 3 min of the cycle). The cation added to SBR1 was Ca^{2+} (i.e., CaCl_2 solution) according to an increase in the supplied Ca/P molar ratio from 2.3 (Table S1) to a mean value of 3.8. The cation added to SBR2 was Mg^{2+} (i.e., MgCl_2 solution) according to an increase in the supplied Mg/P molar ratio from 0.8 (Table S1) to a mean value of 2.3. By the end of this phase, granules >1 mm that accumulated at the bottom of the SBR1 were harvested using a sieve. Finally, in phase IV (simultaneous long-term PNA and HAP precipitation), only Ca^{2+} continued to be added to SBR1, interrupting the Mg^{2+} supply to SBR2. Several pH set-point values were applied within the range 7.0–7.5.

Chemical Analysis, Biological Tests, and Calculations. Offline pH and electrical conductivity (EC) referred to 25 °C were measured with a pH-meter (mod. pH-Meter Basic 20+, Crison

Instruments SA, Spain) and a conductimeter (EC-Meter Basic 30+, Crison Instruments SA), respectively. The TSS were determined gravimetrically after sample filtration and drying to constant weight at 105 °C, and the VSS were measured after further ignition in a muffle furnace at 550 °C. The concentrations of the soluble cations, i.e., ammonium (NH_4^+), sodium (Na^+), potassium (K^+), magnesium (Mg^{2+}), and calcium (Ca^{2+}), as well as the concentrations of the soluble anions, i.e., nitrite (NO_2^-), nitrate (NO_3^-), chloride (Cl^-), sulfate (SO_4^{2-}), and phosphate (PO_4^{3-}), were all determined using ion chromatography (mod. ICS-5000, Dionex), after filtering samples with 0.2 μm nylon filters. The sludge volume index (SVI) was measured in a 1 L graduated cylinder using mixed liquor sampled from the bioreactors at the beginning of a new cycle. The height of the sludge was recorded at different times within an interval of 3–30 min. Thus, the SVI_5 and SVI_{30} were the sludge heights at 5 and 30 min, respectively, per gram of TSS. Before analysis through X-ray diffraction (XRD) (mod. D8 Quest Eco, Bruker), the granular sludge was rinsed with Milli-Q water, filtered, dried, and ground. The chemical composition of this sludge (P, Ca, Mg, and K) was determined by inductively coupled plasma-optical emission spectrometry (ICP-OES) (mod. 5100, Agilent Technologies). Other metals, i.e., arsenic (As), cadmium (Cd), chromium (Cr), copper (Cu), iron (Fe), lead (Pb), mercury (Hg), nickel (Ni), and zinc (Zn), were determined using inductively coupled plasma-mass spectrometry (ICP-MS) (mod. 7500c, Agilent Technologies). The morphology of the granules was qualitatively observed with a stereomicroscope (Stereo Discovery V12, Zeiss), whereas the particle size distribution was studied with a laser diffraction particle size analyzer (LS 13 320, Beckman Coulter), suitable for particle size measurement ranges from 0.040 to 2000 μm .

Nitrogen conversion in the bioreactors was calculated taking into account the concentration of ammonium, nitrite, and/or nitrate in the influent and effluent water lines, as well as the bioreactor working volume and the volumetric flow rate applied. When necessary, results were referred to the suspended solids content in the bioreactor bulk. Short-term specific anammox activity tests were conducted in batch (in duplicates), taking water samples at regular time intervals for subsequent chemical analysis. The supersaturation conditions for particular phosphate mineral phases, i.e., HAP, octacalcium phosphate (OCP, $\text{Ca}_8\text{H}_2(\text{PO}_4)_6 \cdot 5\text{H}_2\text{O}$), tricalcium phosphate (TCP, $\text{Ca}_3(\text{PO}_4)_2$), and MAP ($\text{MgNH}_4\text{PO}_4 \cdot 6\text{H}_2\text{O}$), were assessed through the saturation index (SI, $\log_{10}(\text{IAP}/K_{\text{sp}})$), as a function of the ion activity product (IAP) of the constituent ions and the solubility product constant (K_{sp}) of the mineral phase, using the freeware Visual MINTEQ (ver. 3.1).²⁷ More details regarding this section are given in the Supporting Information.

Microbial Community Analysis by High-Throughput Sequencing. Sludge samples from both bioreactors were collected from the solids' sampling tap (Figure S1) once per month during the first

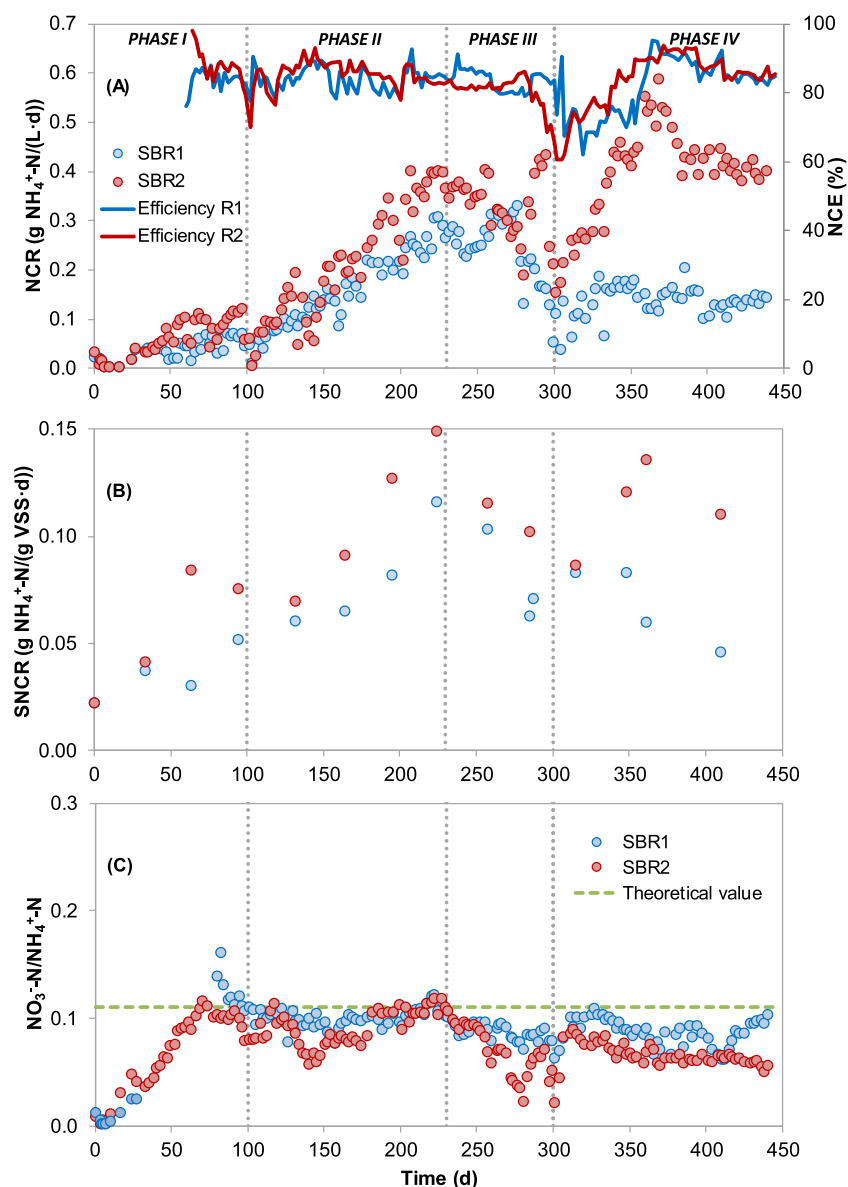


Figure 1. Evolution of the N conversion rate (NCR) and N conversion efficiency (NCE) (A), the biomass specific NCR (SNCR) (B), and the nitrate-produced-to-ammonium-converted ratio (C) in both bioreactors. The theoretical value was assumed as 0.11 mol/mol (see eq 4).

12 months of the experiment to assess the microbial community dynamics. More details regarding the microbial community analysis are given in the [Supporting Information](#). Raw sequence data obtained in this study was deposited at the National Center for Biotechnology Information (NCBI) sequence read archive (SRA) under accession number SUB8280136 and with links to the BioProject database (www.ncbi.nlm.nih.gov/bioproject/) under accession number PRJNA668517.

RESULTS AND DISCUSSION

Performance of Bioreactors. Nitrogen in the Bulk Liquid. The main parameters characterizing the performance of both PNA SBRs during the four operational phases described above (440 days in total) are shown in [Table 1](#) and [Figure 1A–C](#). In phase I, the growth of the granular sludge needed time to consolidate due to the new imposed working conditions and influent wastewater composition, i.e., merging of the seeding sludge coming from two independent full-scale bioreactors into only one lab-scale bioreactor and replacement of the landfill leachate by urban centrate as the feeding stream,

which entailed significant differences in terms of composition and EC (from ca. 35 to 9 mS/cm). In phase II, a progressive increase of the biological activity was achieved—maximum N conversion rates (NCRs) reached by the end of this phase were 0.30 and 0.40 g $\text{NH}_4^+\text{-N}/(\text{L}\cdot\text{days})$ in SBR1 and SBR2, respectively—pushed by the gradual intensification of the aeration rate. The N conversion efficiencies (NCEs) in this phase averaged similarly, i.e., $84 \pm 3\%$ in SBR1 and $85 \pm 4\%$ in SBR2.

In phase III, the addition of a metal ion into the bioreactors did not cause major disturbances during the first part of this phase. In SBR1 (where Ca^{2+} was added), concomitant rates for N conversion and P uptake (PUR) were estimated up to 0.32 g $\text{NH}_4^+\text{-N}/(\text{L}\cdot\text{days})$ and 12 mg $\text{PO}_4\text{-P}/(\text{L}\cdot\text{days})$. On day 285, the purge of the largest granules from SBR1 (7 g of VSS; equivalent to 19% of the total amount of VSS available), together with an intensive maintenance campaign carried out in the experimental setup, caused a drop in the biological activity down to roughly a half. The previous activity achieved

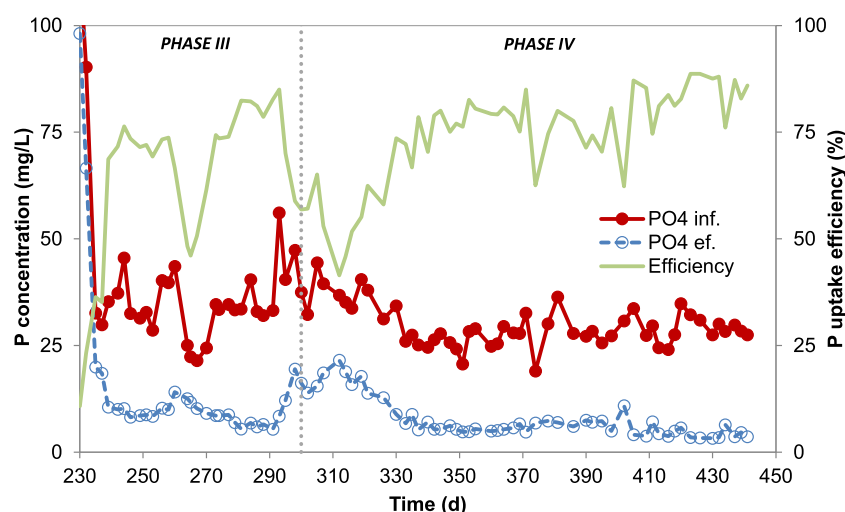


Figure 2. Evolution of the phosphate uptake efficiency in SBR1 while adding Ca^{2+} (phases III and IV).

in this bioreactor was no longer recovered. On the other hand, in SBR2 (where Mg^{2+} was added), higher NCRs were measured initially but without the occurrence of P uptake, similar to that in the previous phase. The maintenance tasks mentioned above also impacted negatively the process performance. Nonetheless, a detrimental effect of Mg^{2+} addition had already been identified a few days before, which will be further discussed later on. Thus, after the initial drop in the biological activity, it progressively recovered in the following weeks, after interrupting the addition of Mg^{2+} and readjusting the aeration rate applied. Values below the expected ones for the PNA process (i.e., 0.11 mol/mol, as shown in eq 4) were confirmed for the nitrate-produced-to-ammonium-converted ratio in both bioreactors, and thus, a slight concomitant heterotrophic denitrification could have been occurring in these systems (favored by the occurrence of cell lysis).

Finally, in phase IV, the NCRs reached were clearly higher in SBR2 (i.e., the maximum measured value was $0.56 \text{ g NH}_4^+ \text{-N}/(\text{L}\cdot\text{days})$) than in SBR1 (i.e., the maximum value in this case was $0.18 \text{ g NH}_4^+ \text{-N}/(\text{L}\cdot\text{days})$). Dependence of the NCE with respect to the pH set-point was confirmed. Thus, the lower the pH set-point value fixed, the higher the NCE attained. As an example, in SBR1, the NCE averaged 72 ± 4 , 84 ± 1 , and $91 \pm 2\%$ in those time intervals when the pH set-points were fixed at 7.5 (days: 312–351), 7.3 (days: 411–440), and 7.0 (days: 364–392), respectively. The switch in the pH set-point value did not imply major changes either in the NCR or in the P-uptake efficiency (PUE).

Phosphorus in the Bulk Liquid. According to the evolution of the concentrations measured in the water line, and favored by the high Ca/Mg molar ratio in the centrate (average: 3.1), in SBR1, CaP formation was expected to occur during most of the experimental period. The intensity of such a process, however, changed with time. In phase II, when the centrate was supplemented with orthophosphate before being fed to the bioreactor (i.e., within the storage tank), the Ca/P molar ratio in the inlet was modified approximately from 2.3 (raw centrate) to 1.3 (expected value after P supplementation). In these circumstances, the concentration of the soluble ion species involved in the precipitation process could fluctuate significantly because crystallization started just after phosphate addition. On the other hand, that fact might imply the addition

of nucleation seeds into the reactor, favoring phosphate precipitation inside. As a rough example for both constituent elements, P and Ca, by considering the 50 days period between days 125 and 175 (in which differences in the mass flow rates between the inlet and the outlet of the bioreactor were more evident), the outflow rates only averaged 78 and 66% of the inflow rates, respectively. On adding Ca to the bioreactor independent of the centrate feeding-in phases III and IV, the concentration of P in the outlet remained lower steadily over time. The PUE reached significantly higher values, of $71 \pm 15\%$ on average, with a maximum as high as 89% in some moments (Figure 2). The drop in the efficiency to about 45% around day 310 was caused by the temporary interruption of Ca supply. On the contrary, in SBR2, no significant phosphate removal from the water line was measured throughout the experimental period, even when Mg addition was implemented in phase III.

Granular Sludge: Solids Content and Specific Activity in the Bioreactors. The observations made using the stereomicroscope evidenced that the sludge that initially inoculated into the bioreactors was formed by red-colored granules surrounded by brown-colored flocculent biomass. This sludge evolved over time toward a brownish and compact structure forming larger granules (Figure S2). The evolution of the size of the particles constituting the biological sludge was also confirmed quantitatively. Thus, the median particle size in the bioreactors once inoculated (day 0) was measured as $84 \mu\text{m}$ (mode $107 \mu\text{m}$; mean: $121 \mu\text{m}$), reaching medians of $380 \mu\text{m}$ in SBR2 and $624 \mu\text{m}$ in SBR1 (modes 431 and $764 \mu\text{m}$; means: 470 and $695 \mu\text{m}$, respectively) after 6 months of running (day 183). By the end of the experimental period (day 440), the median size of the granules was measured as $383 \mu\text{m}$ in SBR2 and only as $296 \mu\text{m}$ in SBR1 (modes 416 and $315 \mu\text{m}$; means: 438 and $328 \mu\text{m}$, respectively), confirming a significant reduction in the case of SBR1. The settling properties of the sludge were assessed throughout the experimental period. The sludge from both bioreactors achieved SVI_{30} values clearly below 70 mL/g TSS and $\text{SVI}_5/\text{SVI}_{30}$ ratios lower than 1.8 (and frequently approaching 1.0–1.2). This is indicative of a very fast settling (sludge settling rates higher than 7 m/h could be reached in the first 3 min) and gives an excellent indication of the presence of dense granules.²⁸ In phases III and IV, the SVI_{30} measured for SBR1

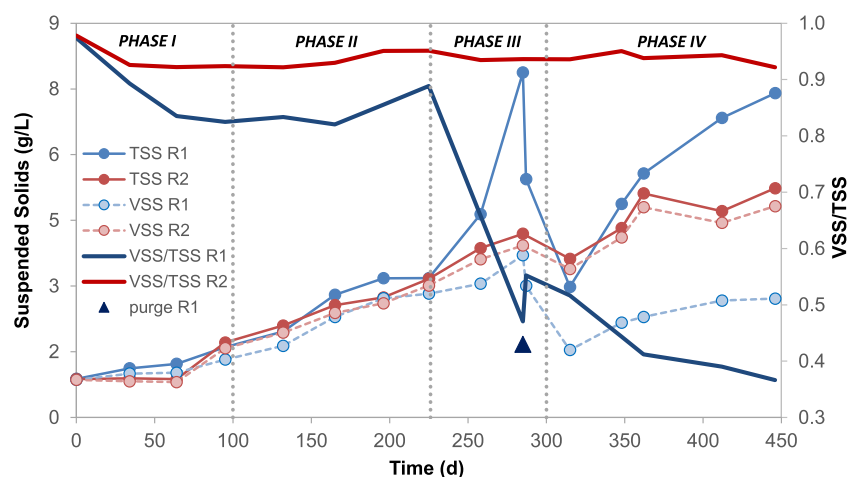


Figure 3. Evolution of the total and volatile suspended solids (TSS and VSS) contents in both bioreactors at the beginning of a new cycle throughout the experimental period.

Table 2. Biological Activity, in Terms of the Specific Nitrogen Conversion Rate (SNCR, g N/(g VSS·days)), Measured in Both PNA SBRs throughout the Experimental Period, According to Their Continuous Performance under Low-Intensity Aeration (On-Site Value), and in Short-Term Batch Incubation Tests Carried Out in Bottles in the Absence of Oxygen to Assess the Specific Anammox Activity (Off-Site Value)^a

bioreactor	SBR1		SBR2	
	on-site	off-site	on-site	off-site
↓ day/value →				
166 (phase II)	0.064 (0.014)	0.109 (0.012)	0.091 (0.009)	0.180 (0.016)
348 (phase IV)	0.083 (0.004)	0.048 (0.006)	0.120 (0.003)	0.195 (0.015)
361 (phase IV)	0.059 (0.008)	0.053 (0.000)	0.135 (0.004)	0.221 (0.002)

^aValues are means (standard deviation (s.d.) in parentheses).

was systematically lower than for SBR2, likely because of the increase in the mineral content (and density) of the sludge. The formation of HAP in the core of the granules, thus, favored the settling of the sludge within the bioreactor (despite the measured decrease in the size of the granules).

In phases I and II, the supplementation of the centrate fed to SBR1 with a phosphate source resulted in the production of granular sludge with a lower organic content (82–97% of the TSS was measured as VSS) than in the case of SBR2 treating raw centrate (92–98%) (Figure 3). By the end of phase II, although similar VSS contents were measured in both SBRs, i.e., ~2.7 g/L by the end of a cycle, different NCRs were determined, i.e., 0.30 g NH₄⁺-N/(L·days) in SBR1 and 0.40 g NH₄⁺-N/(L·days) in SBR2. By adding Ca to SBR1 in phase III, a sharp decrease in the organic content of the sludge was observed; i.e., from 89 to 47% in 60 days. This pattern was not observed in SBR2 after adding Mg for the same period, where the organic fraction of the sludge remained above 90%. At this point (day 285; both bioreactors containing 3.4 g VSS/L), the purge of the largest granules from SBR1 momentarily led to a slight increase in the VSS/TSS ratio of the sludge, but then this ratio continued falling down to a minimum of 37% by the end of phase IV. After 440 days of running, final VSS contents (end of cycle) in SBR1 and SBR2 were measured as 2.6 and 4.3 g/L, respectively.

According to the values determined by the end of phase II, the biological activity in both reactors, referred to as the specific NCR (SNCR), was assessed as 0.116 g NH₄⁺-N/(g VSS·days) for SBR1 and 0.148 g NH₄⁺-N/(g VSS·days) for SBR2 (Table 1). This means a 22% lower rate in the first bioreactor. These were the highest specific rates reached

throughout the experimental period. Smaller values were measured systematically in SBR1, i.e., 10–65% lower rates in comparison to SBR2 (Figure 1B). By the end of phase IV, the SNCR was 59% lower in SBR1 than in SBR2, i.e., 0.045 vs 0.110 g NH₄⁺-N/(g VSS·days). The reduced biological activity of the sludge growing in SBR1 was also confirmed by performing complementary batch incubation tests to assess the specific anammox activity in the short term, as shown in Table 2. For SBR2, the SNCR in such off-site tests was found to be higher than in the bioreactor owing to the strict anoxic conditions imposed. Conversely, this was not always true for SBR1, which might be indicative of some kind of limitation linked to nitrite availability (e.g., related to nitrite mass transfer from the bulk to the mineral-rich inner part of the granule). Concerning P, the maximum PUR measured in SBR1 in phase III, i.e., 12 mg PO₄-P/(L·days), was equivalent to a specific value (specific phosphorus uptake rate (SPUR)) of about 3.8 mg PO₄-P/(g VSS·days).

The presence of divalent metal ions in the bulk liquid of the bioreactors, such as Ca²⁺ and Mg²⁺, promotes granulation by self-immobilization of the individual microbial cells. It is assumed in the literature that the positive charges of these metal ions can partially neutralize the negative charges on the surface of the microbial cells and extracellular polymeric substances (EPS), which mostly consist of polysaccharides and proteins. Both metal ions can help in enhancing the granulation process, favoring the formation of granules with a more compact and dense structure.²⁹ Yet, Ca²⁺ ions preferably bond with polysaccharides, while Mg²⁺ ions preferably bond with proteins, which may affect the characteristics of the granular sludge.³⁰ In the particular case of the

Table 3. Comparison of Some Case Studies Concerning Treatment of Real N-Rich Wastewater in Granular Single-Stage Anammox-Based Systems

reactor type ^a	temperature (°C)	wastewater source	NRR (g N/(L·days))	SNRR (g N/(g VSS·days))	NRE (%)	reference
EGSB	25	digested pig slurry centrate	2.71	0.35	83	Chini et al. ³²
IL-AR	30	digested pig slurry (wastewater)	3.90	0.35	73	Wang et al. ³³
SBR (air pulsing)	21	urban sidestream centrate	0.36	0.10	78	Vázquez-Padín et al. ³⁴
SBR	15–35	urban sidestream centrate	0.30–0.51	0.06–0.11 ^b	81–91	Joss et al. ³⁵
SBR	28	urban sidestream centrate	0.67	0.18	90	Jeaningros et al. ³⁶
SBR	25	urban sidestream centrate	0.27 (SBR1); 0.35 (SBR2)	0.10 (SBR1); 0.13 (SBR2)	75 (SBR1); 73 (SBR2)	this study ^c

^aAbbreviations: EGSB, expanded granular sludge bed; IL-AR, internal loop airlift reactor; NRE, nitrogen removal efficiency; NRR, nitrogen removal rate; SBR, sequencing batch reactor; SNRR, specific NRR; TSS, total suspended solids; VSS, volatile suspended solids. ^bVSS/TSS ratio is assumed as 0.75. ^cValues in terms of conversion rather than removal are (SBR1–SBR2): 0.30–0.40 g N/(L·days); 0.116–0.148 g N/(g VSS·days); and 85–83%.

anammox sludge, protein-type EPS play a major role in cell aggregation.³¹ Thus, in phase III, it is hypothesized that the supply of an extra amount of Mg²⁺ into SBR2 (i.e., the Ca/Mg molar ratio added approximately changed from 3.1 to 1.0; min as 0.5 on day 288) could affect ion interactions with EPS and, finally, granule characteristics and process performance.

The coupling of both partial nitrification (eq 1) and anammox (eq 2) processes in one reactor running under low-intensity aeration led to much lower specific N-removal rates (SNRRs) than those expected in anaerobic reactors specifically dedicated to the anammox process, e.g., 1.10 g N/(g VSS·days), in agreement with the data reported by Strous et al.¹² Yet, values obtained in this study fall within the range of SNRRs (e.g., 0.06–0.35 g N/(g VSS·days)) given in other studies dealing with the treatment of real wastewater in single-stage anammox-based systems (Table 3).^{32–36}

Besides, the results obtained in this study are in line with those from other similar works combining biological N removal and mineral crystallization using mechanically stirred bioreactors. As an example, Sperandio et al.,³⁷ treating synthetic wastewater by nitrification–denitrification in an SBR, showed that phosphate may coprecipitate within the reactor in different forms depending on the pH (7.5–8.5), including both HAP and MAP. More recently, and concerning single-stage PNA systems, Johansson et al.¹⁹ successfully treated real urban sidestream centrate in a granular sludge SBR at 25 °C according to loading rates of 0.31 g N/(L·days) and 18 mg P/(L·days) reaching 66% N removal and HAP recovery without adding chemicals (i.e., wastewater containing 966 mg NH₄⁺–N/L and 57 mg PO₄–P/L; limited details are available about process performance). By switching to synthetic wastewater and an airlift reactor configuration, Guo and Li²³ attained, in a PNA system, removal rates from the water line as high as 1.2 g N/(L·days) and 70 mg P/(L·days) (i.e., wastewater containing 500 mg NH₄⁺–N/L and 20 mg PO₄–P/L). Finally, much higher process rates were reported for simultaneous N removal and P uptake by working with anammox sludge in anaerobic expanded bed reactors fed with synthetic wastewater and running under optimized conditions. In these studies, the NCR (described in terms of N removal) and the PUR (triggering the formation of HAP) from the water line were quantified as high as 16.7 g N/(L·days) and 1.2 g P/(L·days) at 25 °C²² or as 44.8 g N/(L·days) and 0.4 g P/(L·days) at 35 °C.²¹ However, as has been described elsewhere,^{38–40} the accumulation of Ca inside the granules

(mostly as calcium carbonate or CaP) implies an enhancement in their mechanical properties, such as a more rigid structure and a higher strength, but as has also been found in this work, at the cost of losing biological activity.^{23,38,40} These operational parameters affecting biomass growth must be particularly considered in the effort to obtain high PURs. In this regard, the NLR and its relationship with the PLR are meaningful, influencing the amount of sludge produced and its composition. To enhance the handling of the purge of the sludge with respect to what has been done in SBR1, the densest granules might be harvested more regularly from the bioreactor, thus preventing the extraction of large amounts of sludge, for instance, using a hydrocyclone.⁴¹

Composition of the Mineral Phosphate Formed. The mineral fraction of the granular sludge harvested from SBR1 in phase III (Figure 4) was quantified as 53–59% on a dry weight (DW) basis (Figure 3) when the sample was obtained from the solids' sampling tap (see Figure S1). This sludge contained 10.7% (DW) P (Table 4), which is a much higher percentage than typical values of 1–2% in activated sludge or 5–7% in sludge from biological systems dealing with P removal (EBPR) and enriched in polyphosphate accumulating organisms (PAOs).⁴² Otherwise, the P content in the sludge from SBR1 was similar to that reported in previous studies targeting concomitant biological N removal and phosphate precipitation (i.e., 10–16%).^{19,37} The mineral fraction of the sludge raised up to 76% of the DW when only considering those granules that accumulated at the bottom of the bioreactor due to their higher density and which was measured, on a wet weight basis, as 1177 g/L, which is a similar value to that (1135 g/L) reported by Xing et al.⁴⁰ In addition to P, Ca was the other main element constituting the mineral fraction of the granules. If referring to the mineral fraction weight (MW), these two elements accounted for 17.9 and 37.9%, respectively. Other constituent elements of the mineral fraction, such as Mg (0.34%) and K (0.20%), were only found in trace amounts. Hence, the Ca/P molar ratio of the mineral phosphate formed was calculated as 1.64, which is very close to the stoichiometric ratio of 1.67 (i.e., 5/3) for HAP. Moreover, the P content in the mineral fraction was similar to that of the phosphate rock, which typically is 13–17.5%,⁴³ and to the stoichiometric value for HAP, which is 18.5%. The low amount of Mg measured excludes the presence of struvite in any major quantities. The analysis of the crystallographic structure using XRD confirmed

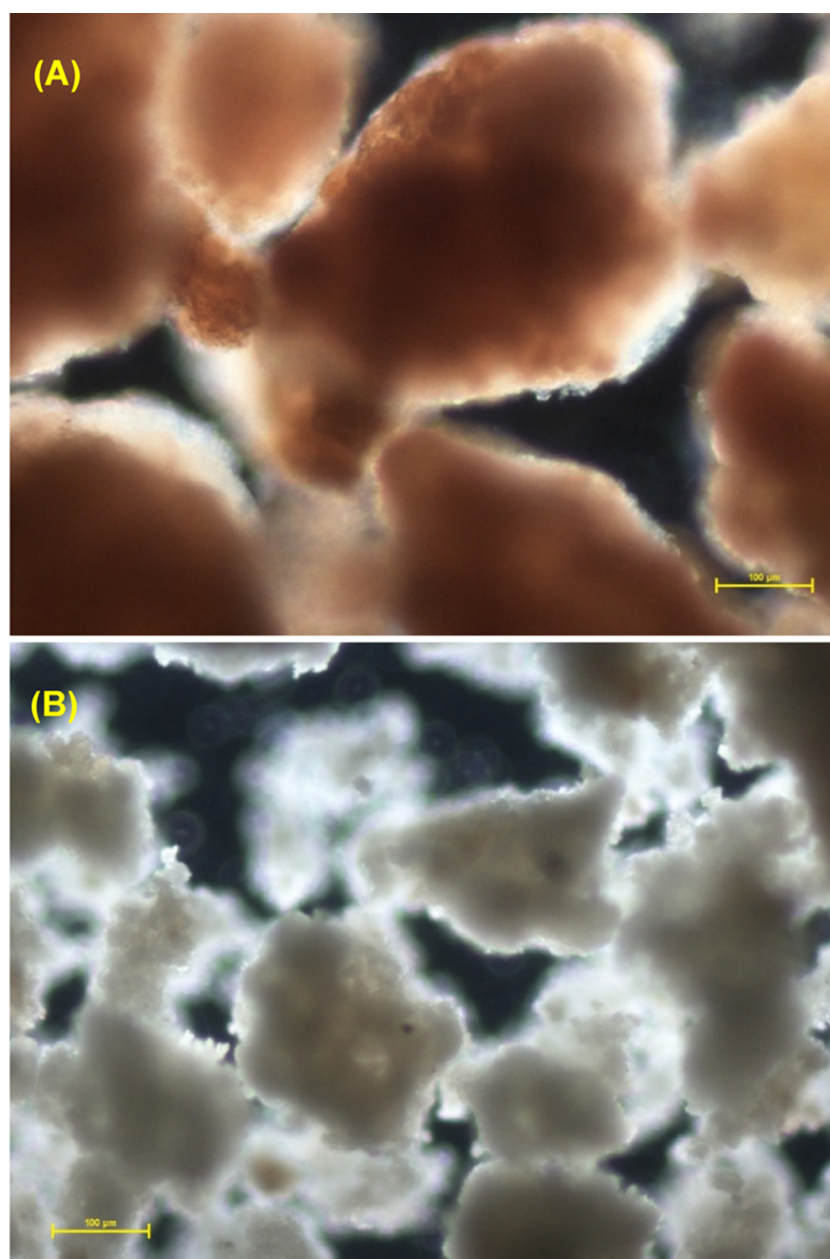


Figure 4. View of the granular sludge growing in SBR1 in phase III (day 285). Fresh sludge (A) and mineral phosphate cores that remained after calcination of the sludge (B).

these results, proving that HAP was the dominant mineral phase (Figure S3).

The presence of metals in the granular sludge formed in SBR1 was quite low, below the proposed EU limits for P fertilizing products⁴⁴—the case of Cr is an exception and could not be assessed since the EU regulation only considers Cr(VI) and the ICP analysis carried out in this study reports total Cr without specifying the oxidation state—and also allowing fulfilling the requirements of the P industry as a raw material.⁴³ The contents of As, Cd, Cr, Cu, Fe, Pb, Hg, Ni, and Zn in the sludge were measured as 13, 0.14, 34, 15, 859, 2.6, 0.53, 14, and 66 mg/kg DW, respectively. This chemical composition is in line with the case study previously reported by Johansson et al.¹⁹ treating similar urban centrate in the same PNA SBR system but without considering the addition of an external Ca source, although the Ni and Pb contents were found to be

clearly higher in this study (roughly about an order of magnitude). Contrary to SBR1, no significant mineral formation was observed in SBR2 throughout the experimental period. If we list the contents in the granular sludge of these nine metals in the same order as above, then the measured values were 12, 0.12, 72, 39, 1743, 22, 1.3, 81, and 135 mg/kg DW, respectively. The higher relative contents of most of the metals in this second case might be justified by the smaller amount of sludge available within the bioreactor acting as a metal accumulator matrix.

The pH of the bioreactor bulk liquid is a key factor affecting the SI of the phosphate mineral phases. Calculations clearly showed that HAP was the mineral phase with the highest SI values (Figure 5), which means that, thermodynamically, it is the most stable phase. This is in line with the results of the XRD and ICP-OES analyses presented for SBR1 (Table 4).

Table 4. Elemental Composition of the Granular Sludge, Determined by ICP-OES^{a,b}

element	SBR1		SBR2		Johansson et al. ¹⁹	
	% DW	% MW	% DW	% MW	% DW	% MW
Ca	22.5	37.9	1.4	22.1	33.5	47.2
P	10.7	17.9	1.3	20.4	15.8	22.3
Mg	0.20	0.34	0.25	3.88	0.24	0.34
K	0.12	0.20	0.21	3.34	0.12	0.17
mineral fraction (% DW)	53–59 (76 if bottom)		6		71 (bottom)	
Ca/P (molar ratio)	1.64		0.84		1.64	

^aComposition is expressed as a percentage of the total dry weight (DW) and as a percentage of the mineral fraction weight (MW).

^bSamples of granular sludge for chemical analysis were obtained from the bioreactor using the solids' sampling tap (see Figure S1).

Yet, besides thermodynamics, kinetics also determine the formation and growth of the crystals. Thus, although HAP can form directly at low phosphate concentrations without any precursors, its formation is normally preceded by the appearance of other more soluble mineral phases, depending on the pH value and the composition of the aqueous solution. In this regard, amorphous calcium phosphate (ACP, $\text{Ca}_3(\text{PO}_4)_2 \cdot x\text{H}_2\text{O}$) has frequently been suggested as the precursor of HAP in granular sludge systems processing wastewater.²⁴ The long retention time of the granules inside the bioreactor will favor the slow transformation of these precursors into HAP, which is the most stable mineral phosphate phase that can be formed, poorly soluble in water. Owing to the fact that ACP (not included in Visual MINTEQ) and TCP have an equivalent Ca/P constituent molar ratio (1.5) and similar K_{sp} , both mineral phases are expected to behave similarly in numerical terms at equilibrium (Figure 5). Otherwise, the SI values calculated for MAP were below those calculated for CaP and lower than zero in the pH range commonly measured in the bulk of the bioreactors (7.0–7.5),

which implies that supersaturation was not reached. This fact points out that the concentration of the constituent ions was too low to cause the precipitation of MAP (even though a raise in the Mg/P molar ratio from 0.7 to 2.3 was assumed in SBR2—phase III). Experimentally for SBR2 (Table 4), the potential existence of a local gradient of pH value within the granule induced by the biological activity was found not to be reason enough to trigger significant HAP or MAP precipitation in its core. At this point, it is worthy to recognize limitations in applying SI calculations to evaluate potential precipitation in complex systems like the one here studied because of the need for appropriate values according to local conditions or the existence of any ion association, complex formation, and hydration in the supersaturated solution.

The formation of HAP in the inner part of the granule (and particularly on the surface of the cell wall—as the site where metabolic fluxes of ions in and out of the cell), rather than in the bulk liquid, has also been reported in other granular PNA systems.^{19,23} In this regard, Guo and Li²³ postulated that, initially, simultaneous growth of microbes and formation of HAP crystals triggers the formation of the sludge aggregates. With the increase in size, mass transfer becomes limiting for the microorganisms growing in the inner part of the particle. Finally, these microorganisms will die and decompose, and the space liberated by them will be occupied by new HAP crystals. Eventual local gradients of pH value (caused by the anammox reaction) and Ca^{2+} ion concentration (which may be influenced by complexation phenomena with negatively charged EPS and microbial cell surfaces) will affect HAP crystallization. The higher the pH value, as well as Ca and phosphate concentrations, the higher the supersaturation reached, benefiting the formation of CaP mineral phases. The availability of carbonate ions may imply competence for the Ca^{2+} ions, affecting negatively the removal of phosphate from the bulk liquid.

Microbial Community Composition and Dynamics.

The final sequence data set consisted of 6 944 738 high-quality reads that, on average, were distributed in 257 213 reads per

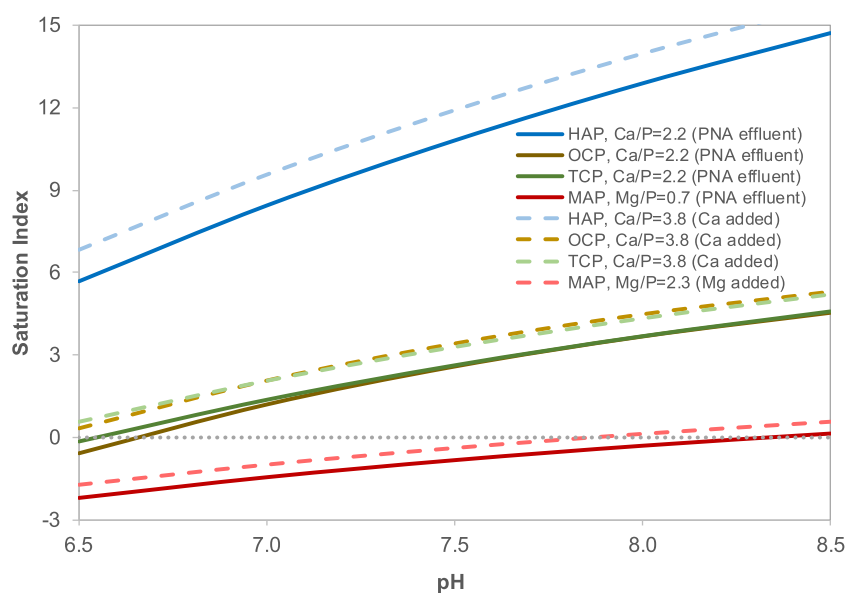


Figure 5. Saturation indexes (SIs) in the bulk of the bioreactor as a function of the pH value for the mineral phases HAP, OCP, TCP, and MAP. Calculations are based on the average concentrations in the effluent from SBR2 in phase II and, when needed, after adjusting the molar ratios by adding the element referred to in the legend.

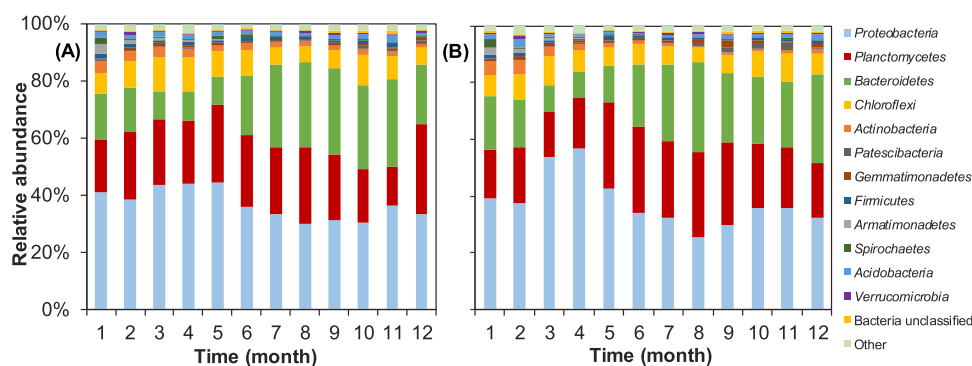


Figure 6. Evolution of the microbial community structure in both SBRs throughout a 12 month experimental period (phase I: months 1–4; phase II: months 5–8; phase III: months 9–10; and phase IV: months 11–12; month 1 is December 2018). The analysis was performed at the phylum level for SBR1 (A) and SBR2 (B). The operational taxonomic units with average relative abundance below 1% were grouped as “other”.

sample (min. = 130 826; max. = 337 792; s.d. = 46 028). This sampling effort was sufficient to recover most of the prokaryotic diversity, as shown in the rarefaction plot (Figure S4).

Microbial Community Diversity and Richness in the Bioreactors. Table S2 shows the α -diversity parameters of the microbial community throughout the bioreactors' operation period. The parameters were calculated after being subsampled in a total of 130 826 sequences and at a distance cutoff level of 0.03. The observed number of operational taxonomic units (OTUs, S_{obs}) varied between 769 and 1235 in SBR1 and between 587 and 1003 in SBR2, showing a lower richness in the latter. The Simpson diversity index ranged from 0.835 to 0.950 in SBR1 and from 0.897 to 0.948 in SBR2, revealing that community diversity was very similar in both reactors. Bottom sludge showed lower diversity (0.835) and lower richness (836 OTUs) than the side sludge sample—i.e., diversity (0.935) and richness (1029 OTUs)—indicating that the bottom sludge corresponds to a mature microbial community, which will be removed from the bioreactors when purging.

Microbial Community Structure and Dynamics in the Bioreactors. The microbial community structure and dynamics were analyzed through the nonmetric multidimensional scaling (NMDS) method (Figure S5). Main process variable vectors were also added in the NMDS space. The ordination of the samples from both SBRs throughout a 12 month experimental period followed a clear trend according to the phases established. Samples concerning phase I (months 1–4) showed large differences among them owing to the fact that, once the bioreactors started running (using as inoculum a mixture of two different sludges, and processing urban sidestream centrate rather than landfill leachate), the growth of the PNA granules required some months to consolidate. From phase II onward (months 5–12), the divergence in the structure of the microbial community gradually increased with respect to the inoculum (month 1) due to its progressive specialization, according to the raise in the NCRs. Maximal divergence was attained at month 12 in SBR1, whereas similar results were obtained at months 11 and 12 in SBR2.

The evolution of the microbial community structure in both bioreactors at the phylum and genus taxonomic levels is shown in Figures 6 and 7. The main phyla in both bioreactors were Proteobacteria, Planctomycetes, and Bacteroidetes, accounting for 37, 23, and 21% of the total sequences (on average), respectively (Figure 6). Also commonly present, although in lower percentages, there were Chloroflexi (8%) and Actino-

bacteria (2%). Other phyla such as Acidobacteria, Armatimonadetes, Firmicutes, Gemmatimonadetes, Patescibacteria, Spirochaetes, and Verrucomicrobia were detected regularly but averaging relative abundances <1%. Planctomycetes, which harbors the AnAOB representatives, reached maximum relative abundances in phase II, when maximum SNCRs were also described (Figure 1B). Bacteroidetes decreased in phase I, from 16 to 10% in SBR1 and from 19 to 9% in SBR2, according to the operational conditions imposed in both bioreactors during the startup. Nevertheless, the relative abundances in the following months rose up to 31 and 32% in SBR1 and SBR2, respectively. These percentages were more fluctuant in SBR2. Although Chloroflexi was not dominant, it was consistently detected in both SBR reactors (maximum relative abundances were measured by the end of phase I, i.e., 12% in SBR1 and 10% in SBR2). Indeed, this phylum is considered to be involved in the stabilization of the granules, as will be discussed further on.

Proteobacteria is one of the main phyla commonly found in N-removal bioreactors, which harbors many nitrifying and denitrifying representatives, and therefore, it is crucial in N-removal processes.^{45–47} The phylum Planctomycetes plays a decisive role in PNA SBRs since it contains all known anammox genera.⁴⁸ Other phyla such as Bacteroidetes and Chloroflexi harbor members potentially capable of facilitating a nitrite loop with AnAOB, or support denitrification, thus contributing to overall N removal in the bioreactors.^{49,50} Moreover, the function of these bacterial phyla in the PNA SBRs is far from being limited to bioconversions within the N-cycle.⁵¹ Thus, for instance, some representatives of both, Bacteroidetes and Chloroflexi, are functionally closely related since both groups include heterotrophic bacteria, which may consume soluble microbial products and EPS, i.e., proteins and polysaccharides, released by the existing microorganisms.^{49,52,53} Moreover, Chloroflexi are filamentous bacteria, which may contribute to the initial formation and further stabilization of the granules⁵³ and benefit from decaying bacterial cell materials according to their heterotrophic metabolism, avoiding the accumulation of bacterial debris and other organic compounds.⁵²

At the genus level, from a total of 1023 taxons retrieved in samples collected from both bioreactors, only 80 (8% of the total) showed relative abundances $\geq 1\%$ (i.e., above 0.55%) in at least one sample. Overall, the dominant genera in both SBRs, showing average percentages above 5%, were *Candidatus Kuenenia* [Planctomycetes] (21%), *Arenimonas* [Gammapro-

(A) ↓ OTU ID / Time (month) →	1	2	3	4	5	6	7	8	9	10	11	12	(B)	1	2	3	4	5	6	7	8	9	10	11	12
Proteobacteria																									
c_ Alphaproteobacteria																									
<i>Brevundimonas</i>	0%	0%	0%	0%	0%	1%	0%	1%	1%	1%	2%	1%	0%	0%	0%	0%	1%	0%	3%	1%	2%	1%	1%	1%	1%
Rhizobiaceae unclassified	2%	1%	0%	1%	1%	1%	0%	0%	0%	0%	0%	0%	2%	1%	1%	1%	1%	1%	0%	0%	0%	0%	0%	1%	0%
Hypomicrobiaceae unclassified	1%	1%	1%	1%	0%	0%	0%	0%	0%	0%	0%	0%	1%	2%	1%	0%	0%	0%	0%	0%	0%	0%	0%	0%	0%
Rhodobacteraceae unclassified	1%	0%	0%	0%	0%	0%	1%	1%	1%	1%	1%	1%	1%	0%	0%	0%	0%	1%	1%	1%	1%	1%	1%	1%	1%
Unclassified	0%	0%	0%	0%	0%	0%	0%	0%	0%	0%	0%	0%	0%	0%	0%	0%	0%	0%	0%	0%	0%	0%	0%	0%	0%
c_ Betaproteobacteria																									
<i>Nitrosomonas</i>	4%	3%	3%	5%	7%	5%	3%	5%	5%	4%	7%	11%	4%	5%	4%	7%	9%	8%	3%	3%	6%	11%	9%	7%	
Burkholderiaceae unclassified	7%	1%	1%	1%	1%	0%	0%	0%	0%	1%	1%	1%	6%	1%	1%	1%	0%	0%	0%	1%	1%	1%	1%	1%	
Ellin6067	0%	0%	0%	0%	0%	0%	0%	0%	0%	0%	1%	0%	0%	0%	0%	0%	0%	0%	0%	0%	0%	0%	0%	0%	
<i>Limnobacter</i>	2%	1%	1%	1%	2%	1%	2%	2%	3%	4%	4%	1%	2%	1%	1%	1%	2%	1%	2%	2%	2%	1%	1%	3%	
<i>Comamonas</i>	1%	2%	2%	2%	1%	1%	1%	1%	1%	1%	1%	0%	1%	1%	2%	1%	2%	1%	1%	1%	1%	0%	0%	1%	
<i>Pusillimonas</i>	2%	0%	0%	0%	0%	0%	0%	0%	0%	0%	0%	0%	3%	0%	0%	0%	0%	0%	0%	0%	0%	0%	0%	0%	
<i>Thiobacillus</i>	0%	0%	0%	0%	0%	0%	2%	2%	1%	0%	0%	0%	0%	0%	0%	0%	1%	1%	1%	1%	1%	0%	0%	0%	
<i>Denitratisona</i>	0%	0%	0%	0%	0%	0%	0%	0%	0%	0%	0%	5%	0%	0%	0%	0%	0%	0%	1%	1%	3%	4%	5%	1%	
c_ Gammaproteobacteria																									
<i>Arenimonas</i>	4%	14%	20%	18%	15%	11%	7%	4%	3%	3%	3%	2%	5%	13%	25%	25%	11%	6%	4%	2%	2%	1%	3%	2%	
<i>Thermomonas</i>	0%	0%	0%	0%	2%	1%	0%	0%	0%	0%	0%	0%	0%	0%	0%	5%	1%	0%	0%	0%	0%	0%	0%	0%	
<i>Dokdonella</i>	1%	1%	2%	2%	2%	1%	1%	1%	1%	1%	0%	0%	0%	1%	3%	2%	2%	1%	1%	0%	0%	0%	0%	1%	
<i>Luteibacter</i>	5%	2%	1%	1%	1%	0%	0%	0%	0%	0%	0%	0%	5%	2%	2%	1%	0%	0%	0%	0%	0%	0%	0%	0%	
<i>Sedimenticola</i>	0%	2%	1%	1%	1%	1%	0%	0%	0%	0%	0%	0%	1%	2%	1%	1%	0%	0%	0%	0%	0%	0%	0%	0%	
PLTA13	0%	0%	0%	1%	1%	3%	4%	5%	4%	5%	5%	3%	0%	0%	0%	1%	2%	3%	4%	5%	4%	4%	5%	5%	
<i>Steroidobacter</i>	2%	1%	2%	1%	2%	2%	2%	1%	1%	1%	1%	0%	2%	1%	2%	2%	2%	2%	1%	1%	1%	0%	0%	1%	
1013-28-CG33	0%	0%	0%	0%	0%	0%	0%	0%	1%	1%	1%	1%	0%	0%	0%	0%	0%	0%	0%	0%	0%	0%	0%	1%	
Unclassified	1%	1%	1%	1%	1%	1%	1%	1%	1%	0%	0%	1%	1%	1%	1%	2%	1%	2%	1%	1%	1%	1%	1%	0%	
c_ Deltaproteobacteria																									
Biri41	0%	1%	1%	1%	0%	1%	2%	1%	1%	1%	1%	1%	0%	2%	2%	1%	1%	2%	2%	1%	1%	2%	2%	2%	
<i>Pajaroellobacter</i>	0%	0%	0%	0%	0%	1%	0%	1%	1%	1%	0%	0%	0%	0%	0%	0%	0%	1%	0%	1%	0%	0%	0%	0%	
0319-6G20	0%	0%	0%	0%	0%	0%	0%	0%	0%	0%	0%	0%	1%	0%	0%	0%	0%	0%	0%	0%	0%	0%	0%	0%	
Syntrophaceae unclassified	0%	0%	0%	0%	0%	0%	1%	0%	0%	0%	0%	0%	0%	0%	0%	0%	0%	0%	0%	0%	0%	0%	0%	0%	
Unclassified	0%	1%	0%	0%	0%	0%	0%	0%	0%	0%	0%	0%	0%	1%	0%	0%	0%	0%	0%	0%	0%	0%	0%	0%	
Planctomycetes																									
f. Brocadiaceae																									
<i>Ca. Kueningenia</i>	16%	21%	21%	18%	21%	23%	22%	26%	22%	18%	12%	29%	15%	17%	14%	15%	28%	28%	25%	28%	27%	21%	20%	18%	
Other																									
<i>Pirellula</i>	0%	0%	0%	1%	3%	0%	0%	0%	0%	0%	0%	0%	0%	0%	0%	0%	1%	1%	0%	0%	0%	0%	0%	0%	
<i>Planctomicrobium</i>	1%	0%	0%	0%	0%	0%	0%	0%	0%	0%	0%	0%	1%	0%	0%	0%	0%	0%	0%	0%	0%	0%	0%	0%	
SM1A02	0%	0%	0%	0%	1%	0%	0%	0%	0%	0%	0%	0%	0%	0%	0%	0%	0%	0%	0%	0%	0%	0%	0%	0%	
S-70	0%	0%	0%	0%	0%	0%	0%	0%	0%	0%	0%	0%	0%	0%	0%	1%	0%	0%	0%	0%	0%	0%	0%	0%	
BD7-11	0%	0%	0%	1%	1%	0%	0%	0%	0%	0%	0%	1%	0%	0%	0%	0%	0%	1%	0%	0%	0%	0%	0%	0%	
Bacteroidetes																									
c_ Ignavibacteriales																									
PHOS-HE36	0%	0%	0%	1%	1%	5%	7%	10%	11%	16%	15%	10%	0%	0%	0%	1%	3%	5%	5%	10%	10%	11%	13%	20%	
<i>Ignavibacterium</i>	0%	0%	0%	0%	0%	2%	3%	0%	0%	0%	0%	0%	0%	0%	0%	0%	0%	2%	1%	1%	0%	0%	0%	0%	
lheB3-7	0%	1%	1%	0%	0%	0%	0%	0%	0%	0%	0%	0%	0%	1%	0%	0%	0%	0%	0%	0%	0%	0%	0%	0%	
c_ Chitinophagales																									
Unclassified 1	10%	5%	1%	1%	0%	1%	7%	3%	4%	2%	1%	0%	12%	8%	1%	0%	0%	0%	4%	6%	3%	1%	0%	0%	
<i>Membranicola</i>	0%	2%	1%	1%	1%	1%	1%	1%	1%	0%	1%	1%	1%	1%	1%	1%	1%	1%	1%	1%	1%	1%	1%	1%	
OLB8	0%	0%	0%	0%	0%	3%	1%	3%	2%	1%	1%	0%	0%	0%	0%	0%	0%	3%	4%	4%	1%	1%	0%	0%	
<i>Phaeodactylibacter</i>	0%	0%	0%	0%	1%	1%	1%	1%	0%	0%	0%	0%	0%	0%	0%	0%	1%	1%	1%	1%	1%	0%	1%	0%	
37-13	0%	1%	0%	0%	0%	0%	0%	0%	0%	0%	0%	0%	0%	0%	0%	0%	0%	0%	0%	0%	0%	0%	0%	0%	
<i>Ferruginibacter</i>	0%	0%	0%	0%	0%	0%	0%	0%	0%	0%	0%	3%	0%	0%	0%	0%	0%	0%	1%	1%	2%	2%	0%	0%	
Chitinophagaceae unclassified	0%	0%	0%	0%	0%	2%	5%	7%	3%	3%	2%	1%	0%	0%	0%	0%	1%	3%	1%	1%	2%	1%	1%	3%	
Unclassified 2	0%	0%	0%	0%	0%	1%	0%	0%	2%	1%	0%	0%	0%	0%	0%	0%	0%	0%	1%	0%	0%	0%	0%	0%	
Other																									
Lentimicrobiaceae unclassified	1%	2%	2%	1%	1%	1%	1%	1%	1%	1%	1%	0%	1%	1%	2%	1%	1%	1%	1%	1%	0%	0%	0%	0%	
AKYH767	0%	0%	0%	0%	0%	0%	0%	1%	1%	1%	1%	0%	0%	0%	0%	0%	0%	1%	1%	1%	1%	1%	1%	1%	
NS11-12 marine group	0%	0%	0%	1%	1%	1%	0%	0%	0%	0%	0%	0%	0%	0%	0%	1%	1%	0%	0%	0%	0%	0%	0%	0%	
env.OPS 17	0%	0%	0%	0%	0%	0%	0%	0%	0%	0%	0%	1%	0%	0%	0%	0%	0%	0%	2%	0%	1%	1%	0%	0%	
NS9 marine group	0%	0%	0%	0%	0%	0%	0%	0%	1%	0%	1%	0%	0%	0%	0%	1%	0%	0%	1%	0%	0%	0%	0%	0%	
<i>Moheibacter</i>	0%	1%	1%	0%	0%	0%	0%	0%	0%	0%	0%	0%	0%	1%	1%	0%	0%	0%	0%	0%	0%	0%	0%	0%	
DMER64	0%	0%	0%	1%	1%	1%	0%	0%	0%	0%	0%	0%	0%	0%	0%	1%	1%	0%	0%	0%	0%	0%	0%	0%	
OPB56	0%	0%	0%	0%	0%	0%	0%	1%	0%	1%	0%	0%	0%	0%	0%	0%	1%	2%	2%	2%	0%	0%	1%	1%	
SJA-28	0%	0%	0%	0%	0%	0%	0%	0%	1%	1%	1%	1%	0%	0%	0%	0%	0%	0%	1%	0%	1%	1%	1%	1%	
<i>Balneola</i>	1%	0%	0%	0%	0%	0%	0%	0%	0%	0%	0%	0%	1%	1%	0%	0%	0%	0%	0%	0%	0%	0%	0%	0%	
Bacteroidia unclassified	1%	0%	0%	0%	0%	0%	0%	0%	0%	0%	0%	0%	1%	0%	0%	0%	0%	0%	0%	0%	0%	0%	0%	0%	
Unclassified	0%	0%	0%	0%	0%	0%	0%	1%	1%	1%	1%	1%	0%	0%	0%	0%	0%	0%	1%	0%	1%	1%	1%	1%	
Chloroflexi																									
SBR1031	3%	5%	7%	6%	5%	5%	3%	2%	2%	4%	3%	2%	3%	5%	5%	4%	3%	4%	3%	2%	2%	4%	4%	2%	
A4b	0%	0%	0%	0%	0%	1%	1%	1%	1%	3%	2%	1%	0%	0%	0%	0%	0%	0%	1%	1%	1%	1%	2%	2%	
OLB14	0%	0%	0%	0%	0%	0%	1%	1%	1%	1%	1%	1%	0%	0%	0%	0%	1%	0%	1%	0%	0%	0%	1%	1%	
JG30-KF-CM66	0%	0%	0%	0%	0%	0%	0%	0%	0%	0%	0%	1%	0%	0%	0%	0%	0%	0%	0%	0%	0%	0%	0%	0%	
Unclassified 1	0%	1%	1%	1%	1%	1%	0%	0%	1%	1%	1%	0%	0%	1%	1%	1%	1%	0%	0%	0%	0%	1%	1%	1%	
Unclassified 2	1%	2%	1%	2%	1%	1%	1%	1%	0%	1%	0%	1%	1%	1%	1%	1%	1%	2%	1%	0%	1%	2%	1%	0%	
Actinobacteria																									
67-14	0%	1%	1%	1%	1%	0%	0%	0%	0%	1%	1%	0%	0%	1%	1%	0%	1%	0%	0%	0%	0%	0%	0%	1%	
IMCC26207	1%	0%	0%	0%	0%	1%	1%	0%	0%	0%	0%	0%	1%	0%	0%	0%	0%	0%	0%	0%	0%	0%	0%	0%	
Actinomarinales unclassified	0%	0%	0%	0%	0%	0%	0%	0%	0%	0%	0%	0%	1%	0%	0%	0%	0%	0%	0%	0%	0%	0%	0%	0%	
Microbacteriaceae unclassified	2%	1%	1%	0%	0%	0%	0%	0%	0%	0%	0%	0%	3%	3%	1%	0%	0%	0%	0%	0%	0%	0%	0%	0%	

Figure 7. continued

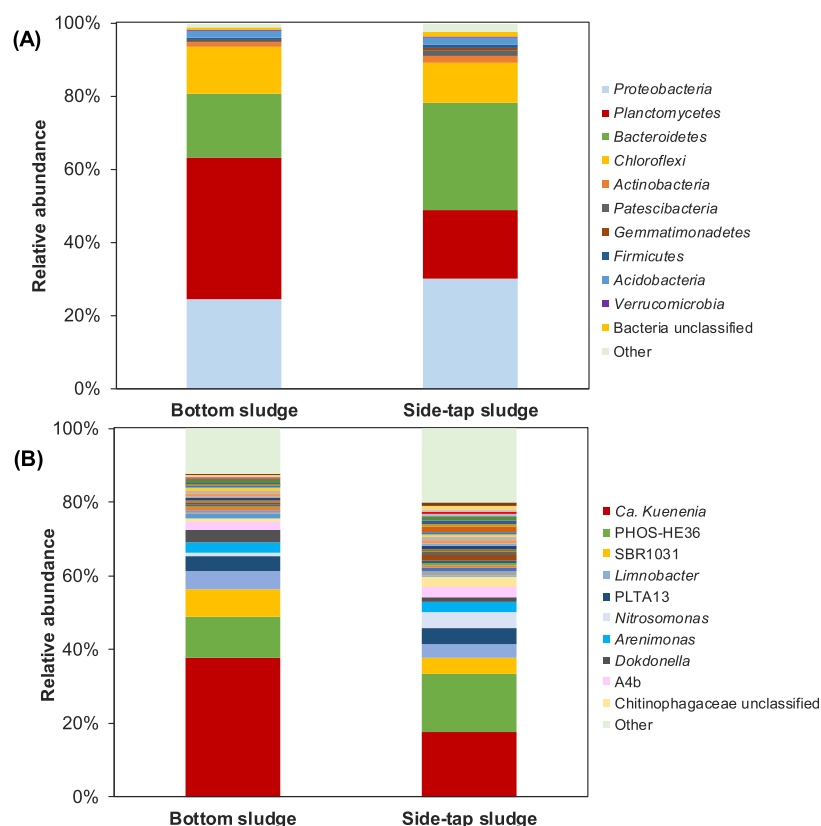


Figure 8. Comparison of the microbial community structure in the granular sludge collected from SBR1 (phase III, month 10, day 285) taking into account samples harvested from the bottom tap (bottom sludge) and from the solids' sampling tap (side-tap sludge). Analysis performed at the phylum (A) and genus (B) levels. The operational taxonomic units (OTUs) with relative abundance <1% were grouped as "other".

percentage regardless of the bioreactor assessed within the range 0.01–0.10%), and *Pseudomonas* (which averaged 0.12% in SBR1—maximum values reached in phase III, but 0.03% in SBR2). In addition, uncultured cyanobacteria belonging to the order *Obscuribacterales* were also detected throughout all of the operational period in both reactors ranging from 0.1 to 0.7% and from 0.1 to 0.4% in SBR1 and SBR2, respectively. These abundances are slightly higher than the 0.1% reported for *Ca. Obscuribacter phosphatis*,⁶¹ which has been recently suggested to play a putative role in EBPR-based processes. Overall, the microbial community analysis reveals that other uncultured bacteria beyond *Ca. A. phosphatis*, including uncultured representatives, might play an important role in P biomineralization as HAP. This result needs to be further addressed in the future by gene expression studies aiming to unravel the identity and the physiological properties of the key organisms favoring HAP formation, which, in turn, will help in enhancing the engineering of the process.

Microbial Community Structure in Different Types of Granules from SBR1. Granules collected from the bottom tap of SBR1 showed a higher density than those collected from the solids' sampling tap (Figure S1) due to the higher mineral content in the core (see the section "Composition of the Mineral Phosphate Formed"). To assess the microbial community structure of both types of granules, sludge samples were taken from both taps in phase III (month 10, day 285). The results showed that the granules from the bottom doubled the relative abundance in anammox taxa (38%) with respect to the granules from the side tap (18%). Also, the percentages for *Nitrosomonas* were lower for the bottom granules (1 vs 4%

for the side-tap granules) (Figure 8). This fact would help in justifying the permanent loss of anammox activity observed after the purge of sludge carried out on day 285, and it is in line with other studies^{12,62,63} stating that the larger (and denser) granules, besides settling faster, harbor larger anoxic volumes, since the oxygen penetration depth is expected to be the same regardless of the size of the granule, which results in favorable conditions for the growth of AnAOB. Otherwise, Bacteroidetes showed a higher relative abundance in the granules from the side tap (29%) than in the granules from the bottom (18%), which agrees with the previously formulated hypothesis that representatives of this phylum contribute significantly to the formation and maturation of the granules. Overall, these results suggest that by an intensive harvesting of the P-rich granules accumulated at the bottom of the SBR1, part of the anammox activity was lost, and the system tended to be more prone to the accumulation of nitrite.

Additional Prospects. In granular sludge PNA systems, the accumulation of HAP for its subsequent valorization as raw material sounds advantageous due to the feasibility of long sludge retention times inside the bioreactor and, once the sludge purged, the possibility for long-term storage before final use. Granules with a mineral HAP core are quite stable and can easily be dehydrated. In contrast to the polyP formed in EBPR systems, where purge of excess sludge needs to be managed appropriately to avoid issues with secondary P release, the precipitated phosphate salts such as HAP are much more stable. However, this study has proved that, although HAP crystallization is compatible with the biological reactions of the PNA process, formation of the mineral phase inside the

granule can significantly reduce the biological activity in the long term. In this regard, a compromise will be needed to balance the interest of extracting HAP-rich granules from the bioreactor, achieving satisfactory N-removal performance. The regular purge of the densest granules formed within the bioreactor would be helpful, avoiding long periods between purges and then proceed to massive sludge discharge. Alternative reactor configurations to SBRs such as the airlift systems have demonstrated good performance regarding the combined PNA + HAP process, reaching higher process rates.²³ On the other hand, the N/P ratio of the wastewater will have an impact on the process, affecting the amount of sludge produced and its composition. The phosphate content in urban sidestream centrates is variable, depending on factors such as the procedure used to achieve P removal in the mainstream (biological vs chemical). Values are normally higher when EBPR-based processes are involved owing to the hydrolysis of the polyP in the anaerobic digester and the consequent release of orthophosphate. For P-rich wastewater, phosphate could finally be precipitated chemically as CaP by adding a Ca source.⁶⁴ If the precipitation takes place at high pH values, outside the optimal pH range for bioprocesses such as PNA, that will make segregated downstream P precipitation necessary. Yet, the high removal of inorganic carbon usually achieved through the PNA process is supposed to facilitate the recovery of phosphate as CaP and help reduce the use of chemicals to modify the pH. According to van der Kooij et al.,⁶⁵ optimized P recovery from sidestream centrate in urban WWTPs will result in modest recovery efficiencies of 3–8% of all P excreted by humans. Other P entering the treatment plant but not recoverable from the centrate will partly be contained in the treated effluent (ca. 20%) and mostly in the dewatered digested sludge (ca. 50–70%). Yet, although P recovery through crystallization from water lines may appear to offer a limited contribution to resolve the global P issues, at a more local scale, such a recovery strategy may offer WWTPs the opportunity of contributing to the creation of more sustainable communities while protecting the environment.

CONCLUSIONS

Feasibility for inducing mineralization of dissolved orthophosphate from urban sidestream centrate in an anammox system running under low-intensity aeration was confirmed. Mineral cores formed inside the granules were mostly composed of HAP (material recoverable as precipitated phosphate salt). The addition of a Ca source helped in enhancing the P-uptake efficiency from the water phase. Yet, the high mineral content of the sludge and its excessive purge from the bioreactor limited the microbial activity in the long term. The densest granules, accumulated at the bottom of the bioreactor, were the richest in HAP but also contained the highest percentages of AnAOB. An operational compromise will thus be needed taking into account the interest of extracting P-rich granules from the system but also the achievement of a satisfactory bioprocess performance.

ASSOCIATED CONTENT

Supporting Information

The Supporting Information is available free of charge at <https://pubs.acs.org/doi/10.1021/acssuschemeng.0c08036>.

Experimental setup (Figure S1); chemical analysis, biological tests, and calculations (Table S1, centrate

characteristics; Figures S2, microscope observations; Figure S3, XRD pattern); and microbial community analysis (Table S2, α -diversity indexes; Figure S4, rarefaction curves; Figure S5, NMDS plots; Figure S6, relative abundances for AOB and AnAOB together with NCR) (PDF)

AUTHOR INFORMATION

Corresponding Author

Albert Magri – LEQUIA, Institute of the Environment, University of Girona, E-17003 Girona, Catalonia, Spain; orcid.org/0000-0002-6993-0746; Phone: +34 972 419 542; Email: albert.magri@udg.edu, albert.magri@gmail.com

Authors

Emma Company – LEQUIA, Institute of the Environment, University of Girona, E-17003 Girona, Catalonia, Spain; orcid.org/0000-0001-7528-9679

Frederic Gich – gEMM, Institute of Aquatic Ecology, University of Girona, E-17003 Girona, Catalonia, Spain; orcid.org/0000-0002-0941-634X

Jesús Colprim – LEQUIA, Institute of the Environment, University of Girona, E-17003 Girona, Catalonia, Spain; orcid.org/0000-0002-6000-069X

Complete contact information is available at: <https://pubs.acs.org/doi/10.1021/acssuschemeng.0c08036>

Notes

The authors declare no competing financial interest.

ACKNOWLEDGMENTS

This research was conducted in the framework of the research project DigesTake (COMRDI16-1-0061) funded by ACCIÓ (Generalitat de Catalunya) within the program Comunitat RIS3CAT Aigua. The group LEQUIA (<http://www.lequia.udg.edu/>) is recognized as a consolidated research group by the Catalan Government (2017-SGR-1552). The authors thank the collaboration of the staff from the company OMS-SACEDE in charge of operating the Terri WWTP (Sunsí Ferrer) and the laboratory work carried out by the students Anastasya Kravtchenko, Guillem Coma, and Mireia Pulido as part of their bachelor's theses at the University of Girona.

ACRONYMS AND ABBREVIATIONS

ACP	amorphous calcium phosphate ($\text{Ca}_3(\text{PO}_4)_2 \cdot x\text{H}_2\text{O}$)
anammox	anaerobic ammonium oxidation
AnAOB	anaerobic ammonium-oxidizing bacteria (anammox bacteria)
AOB	ammonium-oxidizing bacteria
CaP	calcium phosphates
DW	dry weight
EBPR	enhanced biological phosphorus removal
EC	electrical conductivity
EGSB	expanded granular sludge bed
EPS	extracellular polymeric substances
EU	European Union
HAP	hydroxyapatite ($\text{Ca}_{10}(\text{PO}_4)_6(\text{OH})_2$)
IAP	ion activity product
ICP	inductively coupled plasma
IL-AR	internal loop airlift reactor
K_{sp}	solubility product constant

MAP	magnesium ammonium phosphate hexahydrate (struvite, $\text{MgNH}_4\text{PO}_4 \cdot 6\text{H}_2\text{O}$)
MgP	magnesium phosphates
MS	mass spectrometry
MW	mineral fraction weight
NCBI	National Center for Biotechnology Information
NCE	nitrogen conversion efficiency
NCR	nitrogen conversion rate
NLR	nitrogen loading rate
NMDS	nonmetric multidimensional scaling
NOB	nitrite-oxidizing bacteria
NRE	nitrogen removal efficiency
NRR	nitrogen removal rate
OCF	octacalcium phosphate ($\text{Ca}_8\text{H}_2(\text{PO}_4)_6 \cdot 5\text{H}_2\text{O}$)
OES	optical emission spectrometry
OTU	operational taxonomic unit
PAO	polyphosphate accumulating organism
PLR	phosphorus loading rate
PN	partial nitrification
PNA	PN–anammox
PUE	phosphorus uptake efficiency
PUR	phosphorus uptake rate
rRNA	ribosomal ribonucleic acid
SBR	sequencing batch reactor
SNCR	specific nitrogen conversion rate
SNRR	specific nitrogen removal rate
SPUR	specific phosphorus uptake rate
SI	saturation index, $\log_{10}(\text{IAP}/K_{\text{sp}})$
SRA	sequence read archive
SVI	sludge volume index
TCP	tricalcium phosphate ($\text{Ca}_3(\text{PO}_4)_2$)
TSS	total suspended solids
VSS	volatile suspended solids
WWTP	wastewater treatment plant
XRD	X-ray diffraction

REFERENCES

- (1) Cordell, D.; White, S. Peak phosphorus: clarifying the key issues of a vigorous debate about long-term phosphorus security. *Sustainability* **2011**, *3*, 2027–2049.
- (2) Gilbert, N. The disappearing nutrient. *Nature* **2009**, *461*, 716–718.
- (3) EU. *Communication from the Commission to the European Parliament, the Council, the European Economic and Social Committee and the Committee of the Regions on the 2017 List of Critical Raw Materials for the EU*, COM(2017) 490; European Commission: Brussels, Belgium, 2017. <https://ec.europa.eu/transparency/regdoc/rep/1/2017/EN/COM-2017-490-F1-EN-MAIN-PART-1.PDF> (last accessed Dec 18, 2020).
- (4) Carpenter, S. R. Phosphorus control is critical to mitigating eutrophication. *Proc. Natl. Acad. Sci. U.S.A.* **2008**, *105*, 11039–11040.
- (5) Egle, L.; Rechberger, H.; Zessner, M. Overview and description of technologies for recovering phosphorus from municipal wastewater. *Resour., Conserv. Recycl.* **2015**, *105*, 325–346.
- (6) Magrí, A.; Carreras-Sempere, M.; Biel, C.; Colprim, J. Recovery of phosphorus from waste water profiting from biological nitrogen treatment: upstream, concomitant or downstream precipitation alternatives. *Agronomy* **2020**, *10*, No. 1039.
- (7) Römer, W.; Steingrobe, B. Fertilizer effect of phosphorus recycling products. *Sustainability* **2018**, *10*, No. 1166.
- (8) Law, K. P.; Pagilla, K. R. Phosphorus recovery by methods beyond struvite precipitation. *Water Environ. Res.* **2018**, *90*, 840–850.
- (9) Wang, L.; Nancollas, G. H. Calcium orthophosphates: crystallization and dissolution. *Chem. Rev.* **2008**, *108*, 4628–4669.
- (10) Lackner, S.; Gilbert, E. M.; Vlaeminck, S. E.; Joss, A.; Horn, H.; van Loosdrecht, M. C. M. Full-scale partial nitrification/anammox experiences - An application survey. *Water Res.* **2014**, *55*, 292–303.
- (11) Rittmann, B. E.; McCarty, P. L. *Environmental Biotechnology: Principles and Applications*; McGraw Hill Education: Chennai, India, 2012.
- (12) Strous, M.; Heijnen, J. J.; Kuenen, J. G.; Jetten, M. S. M. The sequencing batch reactor as a powerful tool for the study of slowly growing anaerobic ammonium-oxidizing microorganisms. *Appl. Microbiol. Biotechnol.* **1998**, *50*, 589–596.
- (13) Rodriguez-Garcia, G.; Frison, N.; Vázquez-Padín, J. R.; Hospido, A.; Garrido, J. M.; Fatone, F.; Bolzonella, D.; Moreira, M. T.; Feijoo, G. Life cycle assessment of nutrient removal technologies for the treatment of anaerobic digestion supernatant and its integration in a wastewater treatment plant. *Sci. Total Environ.* **2014**, *490*, 871–879.
- (14) Schaubroeck, T.; De Clippeleir, H.; Weissenbacher, N.; Dewulf, J.; Boeckx, P.; Vlaeminck, S. E.; Wett, B. Environmental sustainability of an energy self-sufficient sewage treatment plant: Improvements through DEMON and co-digestion. *Water Res.* **2015**, *74*, 166–179.
- (15) Vlaeminck, S. E.; De Clippeleir, H.; Verstraete, W. Microbial resource management of one-stage partial nitrification/anammox. *Microb. Biotechnol.* **2012**, *5*, 433–448.
- (16) Vangsgaard, A. K.; Mauricio-Iglesias, M.; Gernaey, K. V.; Sin, G. Development of novel control strategies for single-stage autotrophic nitrogen removal: A process oriented approach. *Comput. Chem. Eng.* **2014**, *66*, 71–81.
- (17) Winkler, M. K. H.; Kleerebezem, R.; Kuenen, J. G.; Yang, J.; van Loosdrecht, M. C. M. Segregation of biomass in cyclic anaerobic/aerobic granular sludge allows the enrichment of anaerobic ammonium oxidizing bacteria at low temperatures. *Environ. Sci. Technol.* **2011**, *45*, 7330–7337.
- (18) Simoes, F.; Vale, P.; Stephenson, T.; Soares, A. The role of pH on the biological struvite production in digested sludge dewatering liquors. *Sci. Rep.* **2018**, *8*, No. 7225.
- (19) Johansson, S.; Ruscalleda, M.; Colprim, J. Phosphorus recovery through biologically induced precipitation by partial nitrification-anammox granular biomass. *Chem. Eng. J.* **2017**, *327*, 881–888.
- (20) Ma, H.; Guo, Y.; Qin, Y.; Li, Y.-Y. Nutrient recovery technologies integrated with energy recovery by waste biomass anaerobic digestion. *Bioresour. Technol.* **2018**, *269*, 520–531.
- (21) Zhang, Y.; Ma, H.; Lin, L.; Cao, W.; Ouyang, T.; Li, Y.-Y. Enhanced simultaneous nitrogen and phosphorus removal performance by anammox-HAP symbiotic granules in the attached film expanded bed reactor. *ACS Sustainable Chem. Eng.* **2018**, *6*, 10989–10998.
- (22) Ma, H.; Xue, Y.; Zhang, Y.; Kobayashi, T.; Kubota, K.; Li, Y.-Y. Simultaneous nitrogen removal and phosphorus recovery using an anammox expanded reactor operated at 25 °C. *Water Res.* **2020**, *172*, No. 115510.
- (23) Guo, Y.; Li, Y.-Y. Hydroxyapatite crystallization-based phosphorus recovery coupling with the nitrogen removal through partial nitrification/anammox in a single reactor. *Water Res.* **2020**, *187*, No. 116444.
- (24) Mañas, A.; Pocquet, M.; Biscans, B.; Sperandio, M. Parameters influencing calcium phosphate precipitation in granular sludge sequencing batch reactor. *Chem. Eng. Sci.* **2012**, *77*, 165–175.
- (25) Cunha, J. R.; Tervahauta, T.; van der Weijden, R. D.; Temmink, H.; Hernández-Leal, L.; Zeeman, G.; Buisman, C. J. N. The effect of bioinduced increased pH on the enrichment of calcium phosphate in granules during anaerobic treatment of black water. *Environ. Sci. Technol.* **2018**, *52*, 13144–13154.
- (26) Anfruns, A.; Gabarró, J.; Gonzalez-Olmos, R.; Puig, S.; Balaguer, M. D.; Colprim, J. Coupling anammox and advanced oxidation-based technologies for mature landfill leachate treatment. *J. Hazard. Mater.* **2013**, *258–259*, 27–34.
- (27) Gustafsson, J. P. *Visual MINTEQ*, ver. 3.1; KTH, 2018. <https://vminteq.lwr.kth.se/> (last accessed Dec 18th, 2020).

- (28) Schwarzenbeck, N.; Borges, J. M.; Wilderer, P. A. Treatment of dairy effluents in an anaerobic granular sludge batch reactor. *Appl. Microbiol. Biotechnol.* **2005**, *66*, 711–718.
- (29) Kończak, B.; Karcz, J.; Miksch, K. Influence of calcium, magnesium, and iron ions on aerobic granulation. *Appl. Biochem. Biotechnol.* **2014**, *174*, 2910–2918.
- (30) Sajjad, M.; Kim, K. S. Studies on the interactions of Ca²⁺ and Mg²⁺ with EPS and their role in determining the physicochemical characteristics of granular sludges in SBR system. *Process Biochem.* **2015**, *50*, 966–972.
- (31) Hou, X.; Liu, S.; Zhang, Z. Role of extracellular polymeric substance in determining the high aggregation ability of anammox sludge. *Water Res.* **2015**, *75*, 51–62.
- (32) Chini, A.; Hollas, A. E.; Bolsan, A. C.; Venturin, B.; Bonassa, G.; Cantão, M. E.; Ibelli, A. M. G.; Antes, F. G.; Kunz, A. Process performance and anammox community diversity in a deammonification reactor under progressive nitrogen loading rates for swine wastewater treatment. *Bioresour. Technol.* **2020**, *311*, No. 123521.
- (33) Wang, S.; Wang, L.; Deng, L.; Zheng, D.; Zhang, Y.; Jiang, Y.; Yang, H.; Lei, Y. Performance of autotrophic nitrogen removal from digested piggery wastewater. *Bioresour. Technol.* **2017**, *241*, 465–472.
- (34) Vázquez-Padín, J. R.; Pozo, M. J.; Jarpa, M.; Figueroa, M.; Franco, A.; Mosquera-Corral, A.; Campos, J. L.; Méndez, R. Treatment of anaerobic sludge digester effluents by the CANON process in an air pulsing SBR. *J. Hazard. Mater.* **2009**, *166*, 336–341.
- (35) Joss, A.; Salzgeber, D.; Eugster, J.; König, R.; Rottermann, K.; Burger, S.; Fabijan, P.; Leumann, S.; Mohn, J.; Siegrist, H. Full-scale nitrogen removal from digester liquid with partial nitrification and anammox in one SBR. *Environ. Sci. Technol.* **2009**, *43*, 5301–5306.
- (36) Jeanningros, Y.; Vlaeminck, S. E.; Kaldate, A.; Verstraete, W.; Gravelleau, L. Fast start-up of a pilot-scale deammonification sequencing batch reactor from an activated sludge inoculum. *Water Sci. Technol.* **2010**, *61*, 1393–1400.
- (37) Sperandio, M.; Pambrun, V.; Paul, E. Simultaneous removal of N and P in a SBR with production of valuable compounds: application to concentrated wastewaters. *Water Sci. Technol.* **2008**, *58*, 859–864.
- (38) Ren, T.-T.; Liu, L.; Sheng, G.-P.; Liu, X.-W.; Yu, H.-Q.; Zhang, M.-C.; Zhu, J.-R. Calcium spatial distribution in aerobic granules and its effects on granule structure, strength and bioactivity. *Water Res.* **2008**, *42*, 3343–3352.
- (39) Lin, Y. M.; Lotti, T.; Sharma, P. K.; van Loosdrecht, M. C. M. Apatite accumulation enhances the mechanical property of anammox granules. *Water Res.* **2013**, *47*, 4556–4566.
- (40) Xing, B.-S.; Guo, Q.; Yang, G.-F.; Zhang, Z.-Z.; Li, P.; Guo, L.-X.; Jin, R.-C. The properties of anaerobic ammonium oxidation (anammox) granules: Roles of ambient temperature, salinity and calcium concentration. *Sep. Purif. Technol.* **2015**, *147*, 311–318.
- (41) Bayo, J.; López-Castellanos, J.; Martínez-García, R.; Alcolea, A.; Lardín, C. Hydrocyclone as a cleaning device for anaerobic sludge digesters in a wastewater treatment plant. *J. Cleaner Prod.* **2015**, *87*, 550–557.
- (42) Yuan, Z.; Pratt, S.; Batstone, D. J. Phosphorus recovery from wastewater through microbial processes. *Curr. Opin. Biotechnol.* **2012**, *23*, 878–883.
- (43) Schipper, W. J.; Klapwijk, A.; Potjer, B.; Rulkens, W. H.; Temmink, B. G.; Kiestra, F. D. G.; Lijmbach, A. C. M. Phosphate recycling in the phosphorus industry. *Environ. Technol.* **2001**, *22*, 1337–1345.
- (44) EU. Regulation (EU) 2019/1009 of the European Parliament and of the Council of 5 June 2019 Laying Down Rules on the Making Available on the Market of EU Fertilising Products and Amending Regulations (EC) No 1069/2009 and (EC) No 1107/2009 and Repealing Regulation (EC) No 2003/2003; European Parliament and the Council of the European Union, 2019; pp L 170/1–L 170/114. <http://data.europa.eu/eli/reg/2019/1009/oj> (last accessed Dec 18, 2020).
- (45) Connan, R.; Dabert, P.; Khalil, H.; Bridoux, G.; Béline, F.; Magri, A. Batch enrichment of anammox bacteria and study of the underlying microbial community dynamics. *Chem. Eng. J.* **2016**, *297*, 217–228.
- (46) Gonzalez-Martinez, A.; Rodriguez-Sanchez, A.; Rivadeneyra, M. A.; Rivadeneyra, A.; Martin-Ramos, D.; Vahala, R.; Gonzalez-Lopez, J. 16S rRNA gene-based characterization of bacteria potentially associated with phosphate and carbonate precipitation from a granular autotrophic nitrogen removal bioreactor. *Appl. Microbiol. Biotechnol.* **2017**, *101*, 817–829.
- (47) Akaboci, T. R. V.; Gich, F.; Rusalleda, M.; Balaguer, M. D.; Colprim, J. Assessment of operational conditions towards mainstream partial nitrification-anammox stability at moderate to low temperature: Reactor performance and bacterial community. *Chem. Eng. J.* **2018**, *350*, 192–200.
- (48) van Niftrik, L.; Jetten, M. S. M. Anaerobic ammonium-oxidizing bacteria: unique microorganisms with exceptional properties. *Microbiol. Mol. Biol. Rev.* **2012**, *76*, 585–596.
- (49) Speth, D. R.; in 't Zandt, M. H.; Guerrero-Cruz, S.; Dutilh, B. E.; Jetten, M. S. M. Genome-based microbial ecology of anammox granules in a full-scale wastewater treatment system. *Nat. Commun.* **2016**, *7*, No. 11172.
- (50) Lawson, C. E.; Wu, S.; Bhattacharjee, A. S.; Hamilton, J. J.; McMahon, K. D.; Goel, R.; Noguera, D. R. Metabolic network analysis reveals microbial community interactions in anammox granules. *Nat. Commun.* **2017**, *8*, No. 15416.
- (51) Zhao, Y.; Liu, S.; Jiang, B.; Feng, Y.; Zhu, T.; Tao, H.; Tang, X.; Liu, S. Genome-centered metagenomics analysis reveals the symbiotic organisms possessing ability to cross-feed with anammox bacteria in anammox consortia. *Environ. Sci. Technol.* **2018**, *52*, 11285–11296.
- (52) Kindaichi, T.; Yuri, S.; Ozaki, N.; Ohashi, A. Ecophysiological role and function of uncultured *Chloroflexi* in an anammox reactor. *Water Sci. Technol.* **2012**, *66*, 2556–2561.
- (53) Chu, Z.-r.; Wang, K.; Li, X.-k.; Zhu, M.-t.; Yang, L.; Zhang, J. Microbial characterization of aggregates within a one-stage nitrification-anammox system using high-throughput amplicon sequencing. *Chem. Eng. J.* **2015**, *262*, 41–48.
- (54) Hiras, J.; Wu, Y.-W.; Eichorst, S. A.; Simmons, B. A.; Singer, S. W. Refining the phylum Chlorobi by resolving the phylogeny and metabolic potential of the representative of a deeply branching, uncultivated lineage. *ISME J.* **2016**, *10*, 833–845.
- (55) Quast, C.; Pruesse, E.; Yilmaz, P.; Gerken, J.; Schweer, T.; Yarza, P.; Peplies, J.; Glöckner, F. O. The SILVA ribosomal RNA gene database project: improved data processing and web-based tools. *Nucleic Acids Res.* **2012**, *41*, D590–D596.
- (56) Zhang, L.; Okabe, S. Ecological niche differentiation among anammox bacteria. *Water Res.* **2020**, *171*, No. 115468.
- (57) Dabert, P.; Sialve, B.; Delgenès, J.-P.; Moletta, R.; Godon, J.-J. Characterisation of the microbial 16S rDNA diversity of an aerobic phosphorus-removal ecosystem and monitoring of its transition to nitrate respiration. *Appl. Microbiol. Biotechnol.* **2001**, *55*, 500–509.
- (58) Koenig, A.; Zhang, T.; Liu, L.-H.; Fang, H. H. P. Microbial community and biochemistry process in autotrophic denitrifying biofilm. *Chemosphere* **2005**, *58*, 1041–1047.
- (59) Qiao, S.; Kawakubo, Y.; Cheng, Y.; Nishiyama, T.; Fujii, T.; Furukawa, K. Identification of bacteria coexisting with anammox bacteria in an upflow column type reactor. *Biodegradation* **2009**, *20*, 117–124.
- (60) Zhu, J.; Chen, L.; Zhang, Y.; Zhu, X. Revealing the anaerobic acclimation of microbial community in a membrane bioreactor for coking wastewater treatment by Illumina Miseq sequencing. *J. Environ. Sci.* **2018**, *64*, 139–148.
- (61) Stokholm-Bjerregaard, M.; McLroy, S. J.; Nierychlo, M.; Karst, S. M.; Albertsen, M.; Nielsen, P. H. A critical assessment of the microorganisms proposed to be important to enhanced biological phosphorus removal in full-scale wastewater treatment systems. *Front. Microbiol.* **2017**, *8*, No. 718.
- (62) Bagchi, S.; Lamendella, R.; Strutt, S.; Van Loosdrecht, M. C. M.; Saikaly, P. E. Metatranscriptomics reveals the molecular mechanism of large granule formation in granular anammox reactor. *Sci. Rep.* **2016**, *6*, No. 28327.

(63) Luo, J.; Chen, H.; Han, X.; Sun, Y.; Yuan, Z.; Guo, J. Microbial community structure and biodiversity of size-fractionated granules in a partial nitrification-anammox process. *FEMS Microbiol. Ecol.* **2017**, *93*, No. fix021.

(64) Monballiu, A.; Desmidt, E.; Ghyselbrecht, K.; Meesschaert, B. Phosphate recovery as hydroxyapatite from nitrified UASB effluent at neutral pH in a CSTR. *J. Environ. Chem. Eng.* **2018**, *6*, 4413–4422.

(65) van der Kooij, S.; van Vliet, B. J. M.; Stomph, T. J.; Sutton, N. B.; Anten, N. P. R.; Hoffland, E. Phosphorus recovered from human excreta: A socio-ecological-technical approach to phosphorus recycling. *Resour., Conserv. Recycl.* **2020**, *157*, No. 104744.